Search for GeV Neutrinos from Solar Flares with the IceCube Neutrino Observatory

Author:
Gwenhaël de Wasseige

Advisor:
Prof. Dr. Kael Hanson

Mémoire présenté en vue de l'obtention du diplôme de Master en Sciences Physiques

in the

Interuniversity Institute for High Energies
Département de Physique
Faculté des Sciences
Université Libre de Bruxelles

Academic year 2013 - 2014

À mes grands-parents,

Acknowledgements

The main person I would like to thank is my advisor, Kael Hanson.
I have had the great honour to work with him and this year of master thesis will remain an unforgettable memory. In addition to having taught me everything I know about astroparticle physics, data analysis and programming, he made me realize that I was able to complete this research. His help, his support and his kindness have made that this master thesis is now completed. Kael, I have to thank you more than you think.

Je voudrais également remercier Laurent Favart, directeur de l'Interuniversity Institute for High Energies où ce mémoire a été réalisé. Merci pour les opportunités de conférence et d'école que vous m'avez offertes au cours de cette année. Ce mémoire serait beaucoup moins documenté sans cela.
Merci également à vous ainsi qu'à Stéphane Goriely, pour l'oreille attentive et les commentaires constructifs que vous m'avez apporté.

I would like to thank you Catherine De Clercq, Nick Van Eijndhoven and all the IceCube team of the IIHE - Geraldina, Elisa, David, Thomas, Aongus, Lionel, Martin, Giuliano, Rachel, Jan L. and mainly Krijn - for your support, your help and your advice along the year.

I have to send a very special thank you to Jan Kunnen. Jan, you deserve way more than a thousand CD's for helping me all this year! Thank you for being there for me whenever I called for help!

Merci à Olmo, Mathieu et Maxime pour leur constant soutien, leur écoute et leurs conseils. Notre amitié m'a plus qu'énormément aidé et je vous en remercie grandement!

Merci à Mark Dierckxsens de l'Observatoire Royal de Belgique pour ses références sur les modèles de flux de neutrinos produits dans les éruptions solaires.
Thank you to Giancarlo Brunetti for his references about reconnection models.
Merci à Jean-Marie Frère et Pierre Vilain pour leur aide au sujet de la section efficace des neutrinos.

Enfin je voudrais remercier ma maman, Coline et Jules. Pardon pour toutes ces heures de travail acharné. Je ne vous remercierai jamais assez pour votre patience, votre compréhension et votre soutien.

Contents

List of Figures

Abstract

Since the end of the eighties and in response to an increase in the total neutrino flux in the Homestake experiment, solar neutrino detectors have searched for a solar flare signal. We propose to use IceCube, the South Pole neutrino observatory, to hunt down neutrinos produced in solar flares. IceCube, currently the largest observatory of high energy neutrinos in operation, may be sensitive to this signal and thus permit either a measurement of the signal or more stringent upper limits to be established. Neutrinos from the decay of mesons which are themselves produced in collisions of accelerated protons with the solar chromosphere provide an interesting window into the underlying physics of the acceleration process. This master thesis describes a filtering process and a model-independent analysis of filtered data in order to get this neutrino signal.

Résumé

Depuis la fin des années 80, les détecteurs de neutrinos recherchent, en vain, un signal provenant des éruptions solaires qui confirmerait que l'augmentation du flux total enregistré par l'expérience Homestake est effectivement une conséquence de ces phénomènes solaires magnétiques. Nous proposons d'utiliser IceCube, le détecteur de neutrinos enterré dans la glace du Pôle Sud, pour mettre en évidence ce flux de neutrinos. IceCube, récemment élu "2013 Breakthrough of the Year" par le magazine britannique Physics World, devrait effectivement nous permettre de détecter ce signal ou au moins de fixer une limite supérieure sur le flux de neutrinos venant des éruptions solaires. Ces neutrinos produits par la désintégration des pions résultant de la collision de protons accélérés avec ceux de la chromosphère constitueraient une intéressante fenêtre d'étude des mécanismes d'accélération qui pourraient être impliqués dans les éruptions solaires. Ce mémoire décrit un processus de filtrage ainsi qu'une analyse des données, indépendante des modèles d'accélération proposés par la théorie, dans le but d'extraire ce signal .

Introduction

"I have done a terrible thing :
I have invented a particle that cannot be detected"
W.Pauli, 1930

In 1988, an increase in the overall neutrino flux was measured by the ^{37}Cl collaboration [4]. One of the possible sources for this increase of the neutrino flux are solar flares. Bahcall predicted that if these neutrinos were indeed emitted during the solar flare process, this would lead to large characteristic signals in neutrino detection experiments. Several measurements have been performed after Bahcall's prediction : the SuperKamiokande and SNO results are detailed in section 2.3.To date, no correlation has been found between the measured neutrino flux and solar flares. We propose a search for these solar flare neutrinos using IceCube, the South Pole neutrino observatory.

The first chapter focuses on the neutrino. We start with a historical overview of the neutrino's discovery. A brief description of the Standard Model of particle physics which is the frame in which the neutrino is considered here follows. Although the three light neutrinos have now been discovered, neutrino physics continues to constitute an important field of research. In the near future, the neutrino sector could indeed provide unforeseen results that would push the limits of the Standard Model. This could happen through the study of neutrino oscillations. A description about the oscillation mechanisms is therefore proposed. The two-flavour neutrino oscillations are firstly described in section 1.3.1 followed by an extension to the three-flavour oscillations including a discussion about the mixing parameters in section 1.3.2. The oscillations phenomenon will play an important role in our study. It indeed determines the maximal fraction of the signal we are able to detect at South Pole level.

The second chapter puts the solar flare neutrinos into context. The Sun and its complex magnetic field are briefly described in section 2.1. A description of the solar flares - which are a manifestation of a high density of the magnetic field - directly follows. Flares constitute a way of releasing magnetic energy stored in the corona. This energy is converted into plasma heating and kinetic energy of charged particles. As developed in section 2.2, solar flare neutrinos are produced by the decay of high-energy pions. These pions arise from collisions of accelerated protons with the chromosphere. Neutrinos therefore provide a direct access to hadron acceleration sites in solar flares. This is

the most obvious motivation of the study of solar flare neutrinos. This motivation and a description of previous solar flare neutrino experiments and their results are presented in Section 2.3. Solar flares emit radiations in the entire electromagnetic spectrum. X-rays and γ-rays have a particular interest in our study: the former determine the start time of the flare while the latter, like neutrinos, are a consequence of hadron acceleration. Their production as well as some experiments in charge of their detections are described in section 2.2.

IceCube, awarded the *2013 Breakthrough of the Year* by the British magazine *Physics World*, is described in chapter 3. The energy scale considered in this study - far below the TeV scale of the cosmic neutrinos recently reported in *Science* [16] - compels us to use the detector in a different way. IceCube has been indeed originally designed for studies of high-energy neutrinos. Nevertheless, the South Pole neutrino observatory has a particuliar region dedicated to the low-energy studies : the DeepCore. The entire detector and its main characteristics are explained in 3.3. After a description of neutrino interactions with matter (3.1), the detection principle of underground Cherenkov detector is developed in section 3.2. A discussion about the South Pole ice and its transparency to Cherenkov photons thus allowing detection completes this section. The end of the chapter is dedicated to a comparison between the analysis we carried out and the former solar flare analyses.

Chapter 4 presents the solar flare neutrino analysis that we propose. The evaluation of the sensitivity of our detector to solar flare neutrinos is described in section 4.1. Both Monte Carlo simulations we carried out - a simple and then a sophisticated one - lead to an evaluation of the effective mass of IceCube according to the number of expected solar flare neutrinos, evaluated in the previous section. Section 4.2 explains what we consider as the background of the study and how to get rid of it. A description about the different parameters of filtering directly follows. The fine tuning of parameters' values is then explained. The section ends with the deciding tree of the proposed filtering process. The choice of solar flares constitutes an important step. The reader will indeed see that some assumptions made in the filtering process impose a selection of solar flares. Nevertheless, the same analysis will be carried out - in the near future - using solar flares with another classification. Finally we explain how we analyse the filtered data. As mentioned before, X-rays detection is used as a time-tag in this search for neutrinos.

The last chapter presents the results obtained. Two different point of view have been analysed: each solar flare has first been analysed individually, then, a stacking analysis has been carried out.

Conclusion and outlook finish this master thesis.

Chapter 1

Neutrinos and the Standard Model of Particle Physics

This first chapter presents the theoretical framework in which neutrinos are considered. After a historical overview of neutrino physics, sections 1.2 and 1.3 develop the theoretical characteristics of neutrinos in the Standard Model of particle physics and in its required extensions.

1.1 Neutrinos physics: a historical overview

The first clue of the neutrino's existence was made by J.Chadwick in 1932 [10]. He observed that the energy spectrum of the electron emitted in nuclear beta decay is continuous and not a single peak as expected. This was a puzzling phenomenon which could not be explained by the physics of the time. Later, believing in energy conservation, W.Pauli suggested that it could be the observation of a new particle which escapes detection. In his theory, this particle is electrically neutral and carries away part of the energy in the beta decay process [54]. E.Fermi was the first to develop a theory of radioactive beta decay which included this neutral particle. His origins explain the well-known name of this particle: neutrino or little neutral one in Italian [30].
In 1956, C.Cowan and F.Reines finally observed this particle [20]. Their detector was located 11 meters from a nuclear reactor core and consisted of layers of Cadmium-loaded water used as the neutrino target sandwiched between layers of liquid scintillator observed by photomultipliers. They used the inverse beta decay (IBD) reaction on free protons:

$$\bar{\nu} + p \rightarrow e^{+} + n \tag{1.1}$$

Equation 1.1 is the most favorable reaction to detect reactor neutrinos (actually antineutrinos). IBD has indeed an higher cross section than other reactions such as neutrino-electron scattering as shown in Figure 1.1. Moreover this reaction has a threshold of 1.8 MeV while the neutrinos' spectrum goes up to 8 MeV [6].

The existence of two different kinds of neutrinos was announced in 1962 with the observation of a muon neutrino coming from the pion decay through the weak interaction as in Figure 1.2 [21].
Fifteen years later a new charged leptonic particle, the tau lepton, was discovered implying the existence of a third generation of leptonic particle [56]. In 1991, the L3 detector at the *Large Electron-Positron collider* (LEP) proved that there cannot exist more than three families of light neutrinos, which correspond to the three generations of charged leptonic particles [26]. This was deduced from the width of the Z^0 gauge boson that it has to decay into three different varieties of $\nu - \bar{\nu}$ pairs each contributing 110 MeV to the total width [6]. However the observation of the tau neutrino had to wait until the new millennium and the *Direct Observation of the NU Tau* (DONUT) experiment which observed tau neutrinos in interactions with iron nuclei [39, 65].

Although the three light neutrinos have now been discovered, neutrino physics continues to constitute an important field of research. In the near future, the neutrino sector could indeed provide unforeseen results that would push the limits of the Standard Model. The Standard Model - briefly described in section 1.2 - has had a strong record of success but some questions remain : the strong CP problem, the hierarchy problem or the matter/antimatter asymmetry for example. They led the scientists to think that it could be necessary to develop theories beyond this model. As pointed out by P. Huber - a neutrino theorist and associate physics professor at Virginia Tech - in [60]: *"Studying neutrinos as precisely as we can is a good route. [...] It's clear that neutrinos have been providing us with one surprise after the other."*

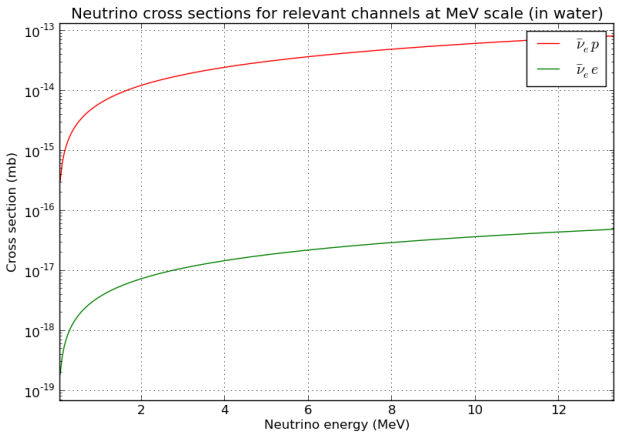

Figure 1.1: Neutrino cross sections for relevant channels at MeV scale. IBD cross section is represented in red while the green stands for the neutrino-electron scattering. Cross sections have been taken in [22].

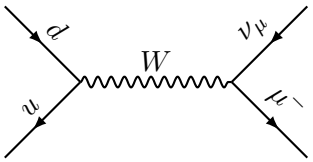

Figure 1.2: The charged pion π^- decay

1.2 The Standard Model of particle physics

The Standard Model of particle physics is the most relevant model describing interactions between particles developed to date. This model is able to describe the properties of elementary particles and their interactions. It contains 12 fermions, their antiparticles and 4 bosons i.e. 3 gauge bosons and the scalar boson (see Figure 1.3) whose interactions are explained through the exchange of the gauge bosons of three of the fundamental forces : the electromagnetic, weak, and strong nuclear interactions. As mentioned above, there are 3 generations of leptonic particles. Each of them contains a charged particle - electron, muon and tau - and the neutrino flavour associated as shown in Table 1.1. These particles turn into another of them by emitting one of the weak bosons: Z^0 and $W^{\pm}$. The Z boson is emitted in a *Neutral Current interaction* (NC) following the channel represented in Figure 1.4 whereas the $W^{\pm}$ is emitted in a *Charged Current interaction* (CC) as shown in Figure 1.5 [29].

Generation	1	2	3
charged	e^-	μ^-	τ^-
neutral	ν_e	ν_μ	ν_τ

Table 1.1: The three generations of leptonic particles.

The neutrino has been originally introduced in the Standard Model of particle physics without mass. However, neutrino experiments highlighted neutrino oscillations - a phenomenon that can only be explained if neutrinos are massive.

In the late 1960's, the Homestake experiment, the first experiment designed to look for solar neutrinos, found too few neutrinos compared to what the Standard Solar Model (SSM) of the time predicted[1]. They called this fact "the solar neutrino problem". The assumption that something was wrong with Davis' experiment disappeared when *Super-Kamiokande* and the Gallium experiments - *SAGE* and *GALLEX* - showed that the model seems to overestimate the solar neutrino capture.

[1] 2.56±0.25 SNU versus 8.1±1.2 SNU where 1 SNU = 10^{-36} neutrino interactions per target atom per second [7].

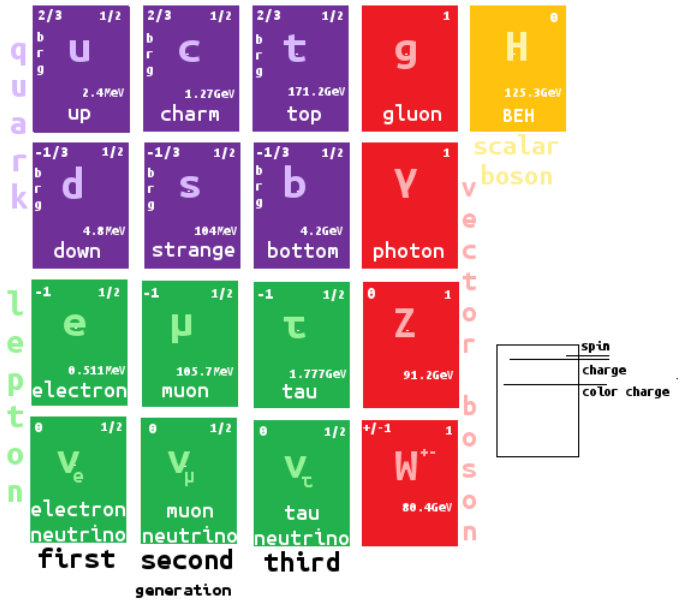

Figure 1.3: The Standard Model of Particle Physics.

Two main reasons could explain these observations :

- The SSM was wrong
- There was something wrong with neutrinos coming from the Sun.

The *Sudbury Neutrino Observatory* (SNO) fixed the problem. This heavy water detector can observe the solar flux in a way that is not dependent on the flavour of the neutrino. It indeed observes the neutral current (NC) channel in addition to the elastic scattering (ES) and the charged current (CC) interactions. Using these three independent channels, SNO was able to give the flux for each neutrino flavour. It found that the total number of $\nu_\mu + \nu_\tau$ is three times higher than the flux of ν_e. Given that the Sun produces only ν_e, the phenomenon of neutrino flavour oscillations was the only possible solution. Moreover, the total flux detected by SNO was in very good agreement with the predictions of the SSM. [27, 7]. More information about the solar neutrino problem but also about the atmospheric neutrino anomaly can be found in [7].

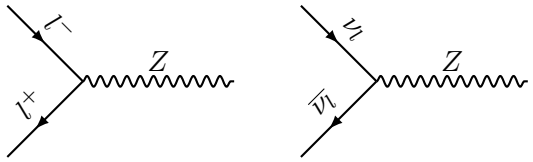

(a) (b)

Figure 1.4: The neutral current interaction. Figure 1.4(a) represents the NC interaction for charged leptons and Figure 1.4(b) is for neutrinos

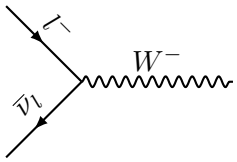

Figure 1.5: The charged current interaction

1.3 Extension of the Standard Model : Neutrino masses and flavour oscillations

It is now a proven fact that neutrinos are massive. There are two different kinds of experiments studying neutrino masses: the direct or the indirect measurement. All direct experiments rely on kinematics variables in $\beta-$decay to deduce the average electron neutrino mass m_{ν_e} in a model-independent way. They study the $\beta-$decay of specific isotopes such as ^3H, ^{187}Re and ^{163}Ho. They can use either a spectrometer either a calorimetric approach. The current upper limit on the neutrino mass m_{ν_e} has been fixed by the ^3H $\beta-$decay experiments at Mainz and Troitsk : $m_{\nu_e} < 2$ eV [35].

The indirect way to prove that neutrino has to be massive consists looking for neutrino flavour oscillations [6].
Neutrino flavour oscillations can be described by standard quantum mechanics. According to these theories if neutrinos oscillate the three mass eigenstates (ν_1, ν_2, ν_3) have to not coincide with the three flavour eigenstates $(\nu_e, \nu_\mu, \nu_\tau)$ which are the weak eigenstates. The two distinct bases are connected by a 3x3 unitary matrix as described in further detail in the following section. We firstly describe two flavour neutrino oscillations and then detail three-flavour-neutrino oscillations.

1.3.1 Two flavour neutrino oscillations

This section is inspired by [7].

In this section we consider two flavours of neutrino. Let's call them ν_α ($\alpha = e, \mu$) with $|\nu_\alpha\rangle$ standing for the weak eigenstates. The energy eigenstates are represented by $|\nu_k\rangle$ (k=1,2) with eigenvalues $E_k = \sqrt{m_k^2 + p^2}$ where p is the momentum and m_k represents the mass of ν_k. This two sets of states are related to each other by an unitary matrix U such as

$$|\nu_\alpha\rangle = \sum_{k=1,2} U_{\alpha k}|\nu_k\rangle \qquad \text{and} \qquad |\nu_k\rangle = \sum_{\alpha=e,\mu} U^*_{\alpha k}|\nu_\alpha\rangle \tag{1.2}$$

or in other words

$$\begin{pmatrix} |\nu_e\rangle \\ |\nu_\mu\rangle \end{pmatrix} = U \begin{pmatrix} |\nu_1\rangle \\ |\nu_2\rangle \end{pmatrix} = \begin{pmatrix} U_{e1} & U_{e2} \\ U_{\mu 1} & U_{\mu 2} \end{pmatrix} \begin{pmatrix} |\nu_1\rangle \\ |\nu_2\rangle \end{pmatrix}$$

Consider a beam of pure ν_α produced at space-time point $(x,t) = (0,0) : |\nu_\alpha(0,0)\rangle$. Let's say that the neutrinos propagate along the x-axis in a free space towards a detector located some distance L away. The propagation of ν_k is given by the time-dependent Schrödinger Equation without potential

$$i\frac{\partial}{\partial t}|\nu_k(x,t)\rangle = E|\nu_k(x,t)\rangle = -\frac{1}{2m_k}\frac{\partial^2}{\partial x^2}|\nu_k(x,t)\rangle$$

whose solutions are plane waves $|\nu_k(x,t)\rangle = e^{-i(E_k t - p_k x)}|\nu_k(0,0)\rangle$ where $p_k = (t, \bar{p})$ is the 4-momentum and $x = (t, \bar{x})$ represents the 4-space vector. At space-time point (x,t), the flavour state $|\nu_\alpha\rangle$ is therefore given by

$$\begin{aligned} |\nu_\alpha(x,t)\rangle &= \sum_{k=1,2} U_{\alpha k}\, |\nu_k(x,t)\rangle \\ &= \sum_{k=1,2} U_{\alpha k}\, e^{-i(E_k t - p_k x)}\, |\nu_k(0,0)\rangle \\ &= \sum_{k=1,2} U_{\alpha k}\, e^{-i(E_k t - p_k x)} \sum_{\gamma=e,\mu} U^*_{\gamma k}\, |\nu_\gamma(0,0)\rangle \end{aligned}$$

where the last equality is obtained from Equation 1.2. Finally

$$\begin{aligned} A(\nu_\alpha(0,0) \to \nu_\beta(x,t)) &= \langle \nu_\beta(x,t)|\nu_\alpha(0,0)\rangle \\ &= \sum_{k=1,2}\sum_{\gamma=e,\mu} U_{\gamma k}\, e^{i(E_k t - p_k x)}\, U^*_{\beta k}\, \langle \nu_\gamma(0,0)|\nu_\gamma(0,0)\rangle \\ &= \sum_{k=1,2} U_{\alpha k}\, e^{i(E_k t - p_k x)}\, U^*_{\beta k} \end{aligned}$$

where $A(\nu_\alpha(0,0) \to \nu_\beta(x,t))$ stands for the transition amplitude for detecting a neutrino of flavour β at space-time (x,t) knowing that a pure ν_α beam was generated in space-time point $(0,0)$. The last step comes from the orthogonality of the flavour states

$\langle \nu_\gamma(0,0)|\nu_\alpha(0,0)\rangle = \delta_{\gamma\alpha}$.
Using the 2x2 rotation matrix as the unitary matrix

$$U = \begin{pmatrix} \cos\theta & \sin\theta \\ -\sin\theta & \cos\theta \end{pmatrix}$$

the amplitude can be easily rewritten such as

$$\begin{aligned}\langle \nu_\beta(x,t)|\nu_\alpha(0,0)\rangle = (&\cos\theta\,\sin\theta\,(e^{i(E_2t-p_2x)} - e^{i(E_1t-p_1x)})\,\langle \nu_\alpha(0,0)| \\ &+ (\sin^2\theta\, e^{i(E_1t-p_1x)} + \cos^2\theta\, e^{i(E_2t-p_2x)})\,\langle \nu_\beta(0,0)|)\,|\nu_\alpha(0,0)\rangle\end{aligned}$$

Remembering that we have a pure ν_α beam at (0,0), the last equation becomes

$$\langle \nu_\beta(x,t)|\nu_\alpha(0,0)\rangle = \cos\theta\sin\theta\,(e^{i(E_2t-p_2x)} - e^{i(E_1t-p_1x)})$$

since $\langle \nu_\beta(0,0)|\nu_\alpha(0,0)\rangle = 0$ and $\langle \nu_\alpha(0,0)|\nu_\alpha(0,0)\rangle = 1$ and the probability of finding ν_β in the pure ν_α beam is just

$$\begin{aligned}P(\nu_\alpha \to \nu_\beta) &= |\langle \nu_\beta(x,t)|\nu_\alpha(0,0)\rangle|^2 \\ &= \cos^2\theta\sin^2\theta\,|(e^{i(E_2t-p_2x)} - e^{i(E_1t-p_1x)})|^2 \\ &= 2\cos^2\theta\sin^2\theta\,(1 - cos(E_2t - p_2x - E_1t - p_1x)) \\ &= \sin^2 2\theta \sin^2\left(\frac{E_2t - p_2x - E_1t - p_1x}{2}\right) \\ &= \sin^2 2\theta \sin^2\left(\frac{(E_2 - E_1)t - (p_2 - p_1)x}{2}\right)\end{aligned}$$

Each step is obtained using either trigonometric identities either a rearrangement. Making the reasonable assumption that the neutrinos are relativistic, $t = x = L$ and

$$p_i = \sqrt{E_i^2 - m_i^2} = E_i\sqrt{1 - \frac{m_i^2}{E_i^2}} \approx E_i\left(1 - \frac{m_i^2}{E_i^2}\right)$$

and assuming that the mass eigenstates are created with either the same momentum or the energy, then

$$(E_2 - E_1)t - (p_2 - p_1)x \approx \frac{\Delta m^2 L}{2E}$$

Substituting back into the probability equation we get

$$P(\nu_\alpha \to \nu_\beta) = \sin^2 2\theta \sin^2\left(\frac{\Delta m^2 L}{4E_\nu}\right) \tag{1.3}$$

The corresponding survival probability is

$$\begin{aligned}P(\nu_\alpha \to \nu_\alpha) &= 1 - P(\nu_\alpha \to \nu_\beta) \\ &= 1 - \sin^2 2\theta \sin^2\left(\frac{\Delta m^2 L}{4E_\nu}\right)\end{aligned}$$

Measuring L in km, E in GeV, replacing $\hbar$ and c and fixing $\alpha = e$ and $\beta = \mu$, we get :

$$P(\nu_e \to \nu_\mu) = \sin^2 2\theta \sin^2 \left(1.27 \left(\frac{\Delta m^2}{1eV^2}\right) \left(\frac{L}{1km}\right) \left(\frac{1GeV}{E_\nu}\right)\right)$$

$$P(\nu_e \to \nu_e) = 1 - \sin^2 2\theta \sin^2 \left(1.27 \left(\frac{\Delta m^2}{1eV^2}\right) \left(\frac{L}{1km}\right) \left(\frac{1GeV}{E_\nu}\right)\right)$$

From the Equation 1.3, it is easy to see that there are two conditions to have neutrino flavour oscillations [68]:

1) the angle θ, which represents the mixing angle, has to be non-zero

2) Δm^2 must be non-zero, which implies that at least one of the mass eigenstates is not identically 0.

The Figure 1.6(a) represents the two last oscillation probabilities for arbitrary E and L. At $L = 0$, the oscillation probability is zero and the corresponding survival probability is one. As L increases, the oscillation probability increases and becomes maximal at $L = 400$km which corresponds to $sin^2\left(\frac{1.27\Delta m^2 L}{E_\nu}\right) = \pi/2$. Then it decreases and gets its minimal value again at $L = 800$km. The Figure 1.6(b) shows oscillations for a wide L range [7].

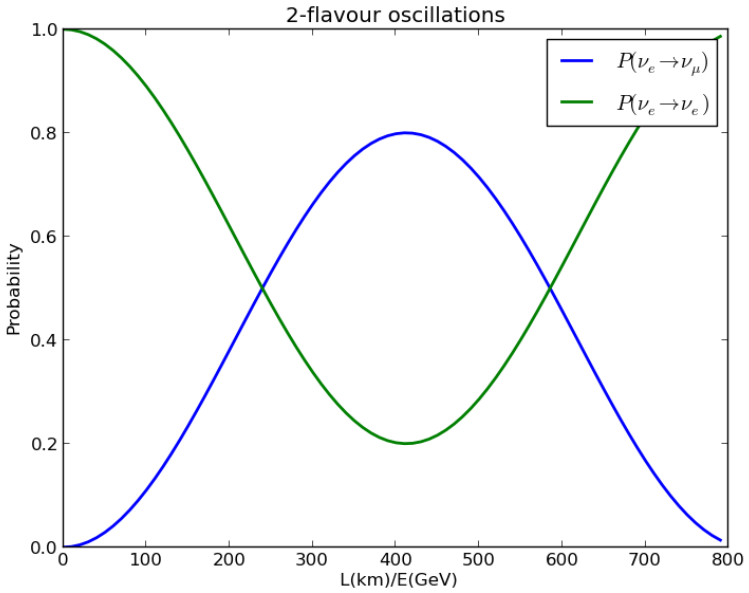

(a)

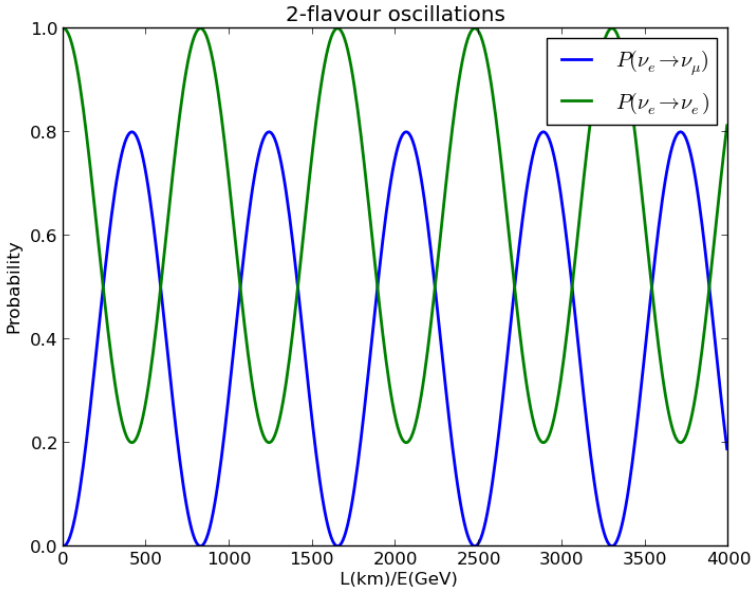

(b)

Figure 1.6: Two flavour neutrino oscillations. The following values have been considered to make the plots : $E = 1$ GeV, $\Delta^2 m = 0.003$ eV^2 and $sin^2 2\theta = 0.8$.

1.3.2 Three flavour neutrino oscillations

Oscillations in vacuum

In the three flavour neutrino oscillations case, things are rewritten as

$$\begin{pmatrix}|\nu_e\rangle\\|\nu_\mu\rangle\\|\nu_\tau\rangle\end{pmatrix} = U\begin{pmatrix}|\nu_1\rangle\\|\nu_2\rangle\\|\nu_3\rangle\end{pmatrix} = \begin{pmatrix}U_{e1} & U_{e2} & U_{e3}\\U_{\mu1} & U_{\mu2} & U_{\mu3}\\U_{\tau1} & U_{\tau2} & U_{\tau3}\end{pmatrix}\begin{pmatrix}|\nu_1\rangle\\|\nu_2\rangle\\|\nu_3\rangle\end{pmatrix}$$

The 3x3 unitary mixing matrix U, which can be complex, is known as the Pontecorvo-Maka-Nakagawa-Sakata (PMNS) matrix. It is the equivalent in the neutrino sector than the CKM in the quark sector. The unitarity condition implies

$$\begin{pmatrix}|\nu_1\rangle\\|\nu_2\rangle\\|\nu_3\rangle\end{pmatrix} = U^\dagger\begin{pmatrix}|\nu_e\rangle\\|\nu_\mu\rangle\\|\nu_\tau\rangle\end{pmatrix} = \begin{pmatrix}U^*_{e1} & U^*_{\mu1} & U^*_{\tau1}\\U^*_{e2} & U^*_{\mu2} & U^*_{\tau2}\\U^*_{e3} & U^*_{\mu3} & U^*_{\tau3}\end{pmatrix}\begin{pmatrix}|\nu_e\rangle\\|\nu_\mu\rangle\\|\nu_\tau\rangle\end{pmatrix}$$

A similar development than the one made for two flavour neutrino oscillations, starting with a pure $|\nu_\alpha\rangle$ state

$$|\psi(x=0)\rangle = U_{\alpha1}|\nu_1\rangle + U_{\alpha2}|\nu_2\rangle + U_{\alpha3}|\nu_3\rangle$$

leads to

$$\begin{aligned}|\psi(L)\rangle = &\left(U_{\alpha1}U^*_{e1}e^{-i(E_1t-p_1x)} + U_{\alpha2}U^*_{e2}e^{-i(E_2t-p_2x)} + U_{\alpha3}U^*_{e3}e^{-i(E_3t-p_3x)}\right)|\nu_e\rangle\\ &+\left(U_{\alpha1}U^*_{\mu1}e^{-i(E_1t-p_1x)} + U_{\alpha2}U^*_{\mu2}e^{-i(E_2t-p_2x)} + U_{\alpha3}U^*_{\mu3}e^{-i(E_3t-p_3x)}\right)|\nu_\mu\rangle\\ &+\left(U_{\alpha1}U^*_{\tau1}e^{-i(E_1t-p_1x)} + U_{\alpha2}U^*_{\tau2}e^{-i(E_2t-p_2x)} + U_{\alpha3}U^*_{\tau3}e^{-i(E_3t-p_3x)}\right)|\nu_\tau\rangle\end{aligned}$$

Then, the oscillation probability is

$$\begin{aligned}P(\nu_\alpha\to\nu_\beta) &= |\langle\nu_\beta|\psi(L)\rangle|^2\\ &= \left(U_{\alpha1}U^*_{\beta1}e^{-i(E_1t-p_1x)} + U_{\alpha2}U^*_{\beta2}e^{-i(E_2t-p_2x)} + U_{\alpha3}U^*_{\beta3}e^{-i(E_3t-p_3x)}\right)^2\end{aligned}$$

Using the unitarity of U and the fact that $Re(U^*_{\alpha i}U_{\beta i}U_{\alpha j}U^*_{\beta j})$ is symmetric and $Im(U^*_{\alpha i}U_{\beta i}U_{\alpha j}U^*_{\beta j})$ antisymmetric under the interchange of i and j, we get

$$\begin{aligned}P(\nu_\alpha\to\nu_\beta) &= \delta_{\alpha\beta} - 4\textstyle\sum_{i>j} Re(U^*_{\alpha i}U_{\beta i}U_{\alpha j}U^*_{\beta j})\sin^2(\Delta m^2_{ij}\frac{L}{4E})\\ &\quad +2\textstyle\sum_{i>j} Im(U^*_{\alpha i}U_{\beta i}U_{\alpha j}U^*_{\beta j})\sin(\Delta m^2_{ij}\frac{L}{2E})\end{aligned} \tag{1.4}$$

Let's go back to the PMNS matrix which can be seen as three rotations matrices and a complex phase :

$$U = \begin{pmatrix}1 & 0 & 0\\0 & c_{23} & s_{23}\\0 & -s_{23} & c_{23}\end{pmatrix}\begin{pmatrix}c_{13} & 0 & s_{13}\,e^{i\delta}\\0 & 1 & 0\\-s_{13}\,e^{i\delta} & 0 & c_{13}\end{pmatrix}\begin{pmatrix}c_{12} & s_{12} & 0\\-s_{12} & c_{12} & 0\\0 & 0 & 1\end{pmatrix}$$

Multiplying matrices, we get :

$$U = \begin{pmatrix} c_{12}c_{13} & s_{12}c_{13} & s_{13}e^{-i\delta} \\ -s_{12}c_{23} - c_{12}s_{23}s_{13}e^{i\delta} & c_{12}c_{23} - s_{12}s_{13}s_{23}e^{i\delta} & c_{13}s_{23} \\ s_{12}s_{23} - c_{12}s_{13}c_{23}e^{i\delta} & -c_{12}s_{23} - s_{12}s_{13}c_{23}e^{i\delta} & c_{13}c_{23} \end{pmatrix} \tag{1.5}$$

where $c_{ij} = \cos\theta_{ij}$ and $s_{ij} = \sin\theta_{ij}$

If we fix the CP phase $\delta = 0$. We therefore lose the imaginary part and we get for the oscillation probability, replacing c and $\hbar$ and assuming $\beta \neq \alpha$,

$$\begin{aligned} P(\nu_\alpha \to \nu_\beta) = &- 4\sum_{i>j}(U_{\alpha i}U_{\beta i}U_{\alpha j}U_{\beta j})\sin^2(1.27\Delta m^2_{ij}\frac{L}{E}) \\ &= -4[(U_{\alpha 1}U_{\beta 1}U_{\alpha 2}U_{\beta 2})\sin^2(1.27\Delta m^2_{12}\frac{L}{E}) \\ &+ (U_{\alpha 1}U_{\beta 1}U_{\alpha 3}U_{\beta 3})\sin^2(1.27\Delta m^2_{13}\frac{L}{E}) \\ &+ (U_{\alpha 2}U_{\beta 2}U_{\alpha 3}U_{\beta 3})\sin^2(1.27\Delta m^2_{23}\frac{L}{E})] \end{aligned}$$

Note that we have the condition

$$\Delta m^2_{12} + \Delta m^2_{13} + \Delta m^2_{23} = 0$$

This probability can be split in two cases as shown in detail [7]. The oscillation and survival probabilities for each flavour are illustrated in Figure 1.9.

If the CP phase $\delta \neq 0$. The imaginary part of Equation 1.5 is not zero. The sign will change for antineutrinos. Therefore, $P(\bar{\nu}_\alpha \to \bar{\nu}_\beta) \neq P(\nu_\alpha \to \nu_\beta)$. The CP conservation is violated and the lepton sector displays matter-antimatter asymmetry such as the quark sector [71].

The mass hierarchy Experiments designed to study neutrino oscillations can only give values for Δm^2_{ij} and not for the individual masses. The Δm^2_{ij} imply either a spectrum of m^2 eigenstates as in Figure 1.7 or either what we will call the inverted hierarchy i.e. m^2_1 and m^2_2 heaviest than m^2_3 [71].

Majorana neutrinos This discussion has been developed for Dirac particles. If neutrinos are Marojana particles which means that they are their own antiparticles, we have to adjust the mixing matrix U. A 3x3 unitary matrix is indeed specified by 9 parameters but can be redefined and characterized by 9 - 3 = 6 parameters by absorbing phase factors into the definition of the lepton fields. The Dirac mixing matrix 1.2 has

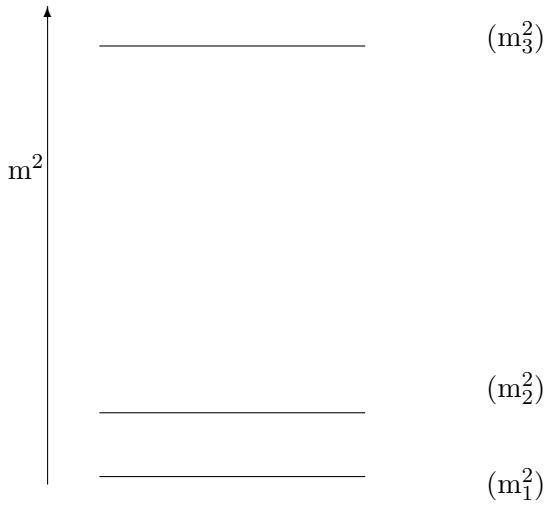

Figure 1.7: One of the two possible mass hierarchies

4 parameters. An extension including two more parameters is therefore required. One may take

$$U_{\text{Majorana}} = U_{\text{Dirac}} \times \begin{pmatrix} 1 & 0 & 0 \\ 0 & e^{i\frac{\alpha_{21}}{2}} & 0 \\ 0 & 0 & e^{i\frac{\alpha_{31}}{2}} \end{pmatrix}$$

where the Majorana angles α_{21} and α_{31} are two additional CP phases. However, they do not contribute to the CP violation of the neutrino oscillations. It can indeed be demonstrated that $U^M_{\beta j} U^{M*}_{\alpha j} = U^D_{\beta j} U^{D*}_{\alpha j}$. Majorana nature of neutrinos would be highlighted by the observation of neutrinoless double beta decay. This subject goes far beyond the scope of this analysis but detail can be found in [71].

Oscillations in matter

It is common to use the Mikheyev, Smirnov and Wolfenstein (MSW) mechanism to study oscillations in matter. Oscillations in matter will play an important role in the search for neutrinos coming from solar flares from the far side of the Sun. These neutrinos have indeed to cross the Sun before reaching the Earth. This analysis is essential to complete the study of neutrinos coming from solar flares. It will be realized in the future. Information about this mechanism can be found in the Appendix D of [55].

Experimental results

The free parameters have been constrained by various experiments: Δm_{12} and θ_{12} from measurements of the solar neutrino fluxes [70]; Δm_{23} and θ_{23} from atmospheric neutrinos [28]. Some people used to make the approximation $s13 = 0$. The analyses were therefore greatly simplified since the number of participating neutrino mass eigenstates is reduced from three to two. This approximation eliminates the possibility of leptonic CP violation as it can be seen in the mixing matrix in Equation 1.5[2]. Several experiments have recently reported non-zero measurements of θ_{13} as for example T2K, MINOS, RENO and Double Chooz [3]. A summary of results is shown in Figure 1.8. The approximation $s13 = 0$ is so no longer valid. Detail can be found in [62, 24]. The current experimentally determined values of the oscillation parameters are given in Table 1.2.

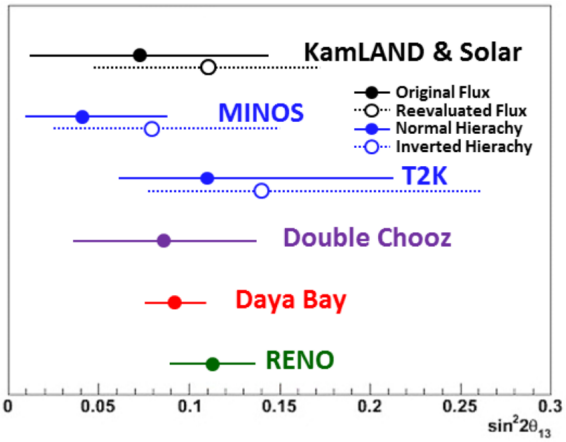

Figure 1.8: Summary of $\sin^2 2\theta_{13}$ values as of May 2012 [62].

[2] U_{e3} becomes zero in this approximation

[3] T2K and MINOS are long-baseline detectors and RENO, Double Chooz and DayaBay are reactor experiments. Detail in [62, 24].

$\sin^2\theta_{12}$	$0.307^{+0.018}_{-0.016}$	
$\sin^2\theta_{23}$	$0.386^{+0.024}_{-0.021}$	$(0.392^{+0.039}_{-0.022})$
$\sin^2\theta_{13}$	0.0241 ± 0.0025	$(0.0244^{+0.0023}_{-0.0025})$
Δm^2_{12}	$7.54^{+0.26}_{-0.22}10^{-5}$ eV^2	
$\lvert\Delta m^2_{23}\rvert$	$2.43^{+0.06}_{-0.10}10^{-3}$ eV^2	$(2.42^{+0.07}_{-0.11}10^{-3}$ eV$^2)$

Table 1.2: Current values of oscillation parameters. These values come from the update version from May 2013 of the Particle Data Group [28]. Values in bracket correspond to the inverted hierarchy case.

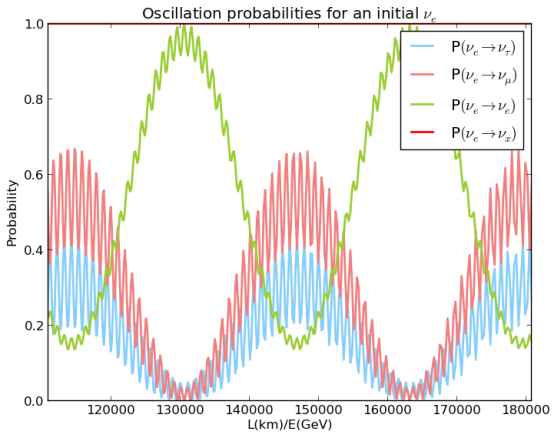

(a)

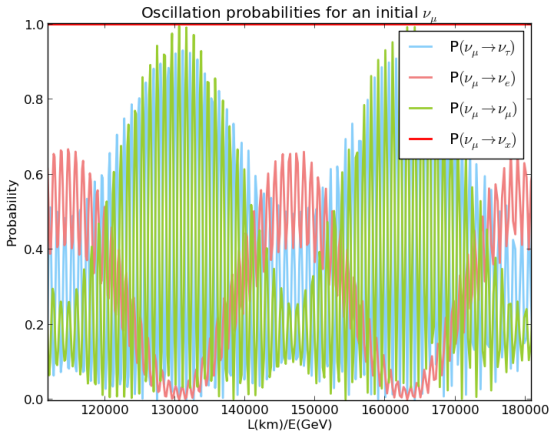

(b)

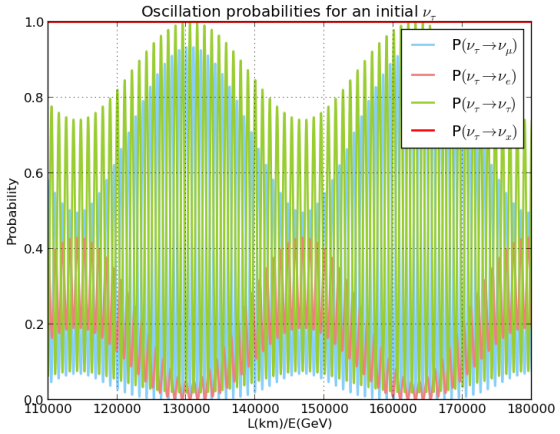

(c)

Figure 1.9: Three flavour neutrino oscillations. Figure 1.9(a) is obtained assuming a pure ν_e beam at (0,0). Figures 1.9(b) and 1.9(c) are respectively for a pure ν_μ and a pure ν_τ at (0,0).

Chapter 2

Neutrinos and Solar Flare Physics

This chapter is dedicated to illustrate the characteristics and the interest of neutrinos in solar flare physics. After a short introduction about the Sun and some of the characteristics of its magnetic field, the first section focuses on the description of solar flares. The second section describes neutrino production as well as the information that neutrinos could bring. Section 2.3 finally explains the state of the art in this search for neutrinos.

2.1 The Sun

The Sun is located at an average distance from Earth which defines the astronomical unit i.e. $1\,\mathrm{UA} = 149,597,870,700$ m [3]. This distance varies depending on the time of year (see consequences in Section 5.1). The Sun is composed of different layers called - from the center to the outer part :

- the core
- the radiative zone
- the convective zone
- the photosphere
- the chromosphere
- the transition region
- the corona

The Sun has a complex magnetic field which follows an 11-year-cycle. It leads to the solar activity which includes sunspots at the solar surface, solar flares and variations in solar wind. Although a discussion about the radiative and convective zone could be interesting in this topic because they are believed to be the place where the magnetic field is produced through a magnetic solar dynamo, we do not explain more about them here. Information can be found in [53]. The chromosphere and transition region

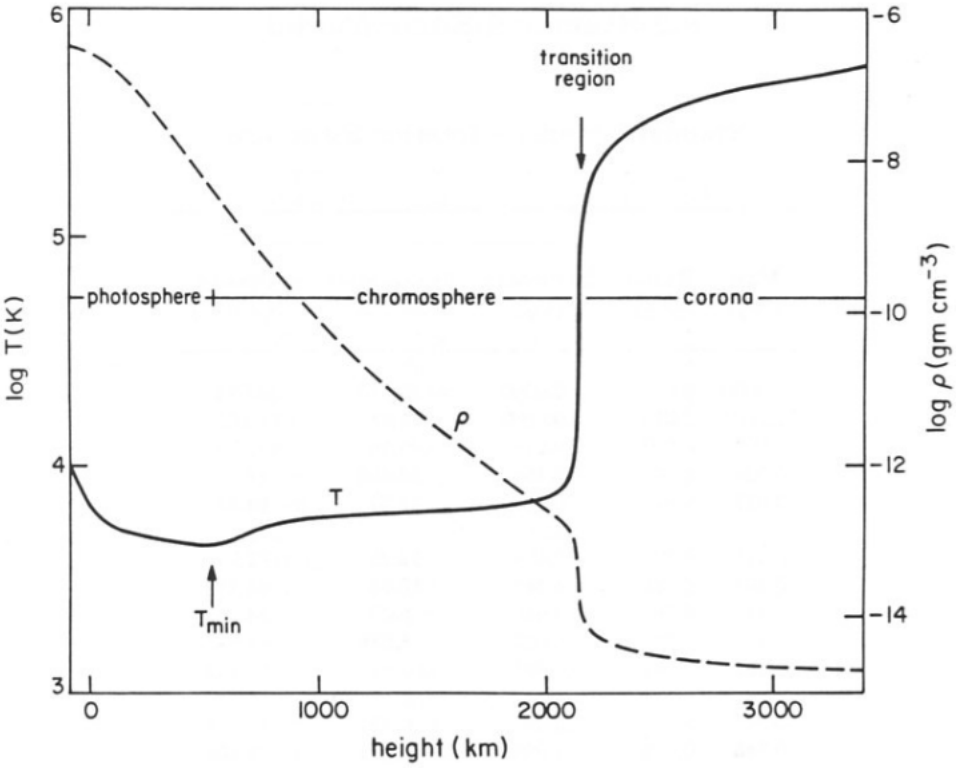

Figure 2.1: Temperature and density functions versus the height above the photosphere [25].

are the most interesting regions in this study. As explained in Section 2.2.2, they are the site of neutrino production. The chromosphere, located above the photosphere, is characterized by a positive temperature gradient: from 4000 K to about 20,000 K with a gradual increase. This atmosphere layer is some ten to fifteen thousand kilometres thick. The temperature in the transition region meanwhile rises up to 1,000,000 K in about 120 km. Figure 2.1 show the temperature and density functions versus the height above the photosphere [25, 2]. More information about chromosphere in solar flare physics can be found in [48].

2.1.1 Sunspots

Sunspots are dark circles visible on the Sun's surface shown in Figure 2.3. They are located in the photosphere and give an evidence of the high magnetic field concentration at this point. Although Galileo had already noted the existence of the sunspots with his telescope, the 11-solar-cycle which domines the number of sunspots has been highlighted much later - in 1755 - by R.Wolf [41]. Figure 2.2 shows the current cycle - i.e. the 24th since 1955 - and the prediction of the end of cycle [2].

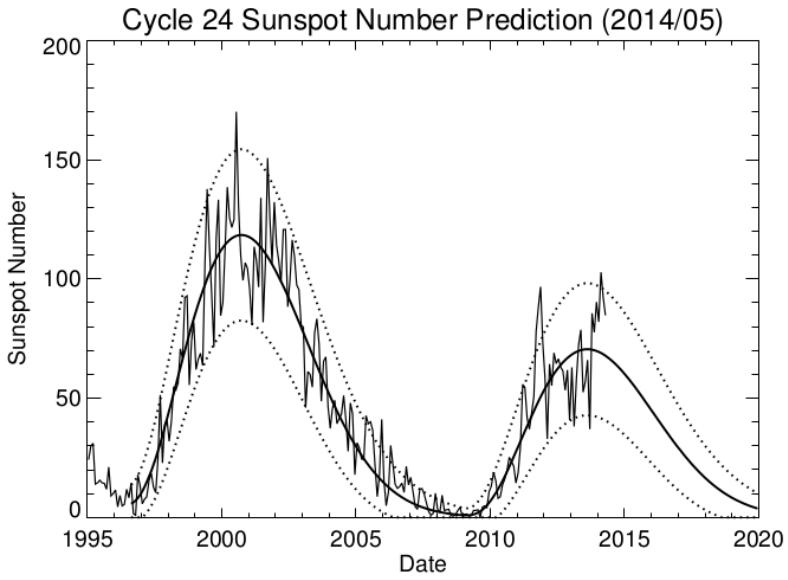

Figure 2.2: Solar cycle prediction - update 2014/05. The sunspot number is given by the sum of the individual sunspots and ten times the number of clusters. Even if conditions of observation are not ideal or small sunspots are hard to see, this formula is able to give reliable numbers. The monthly averages are shown in this figure [2]. Image credit: NASA

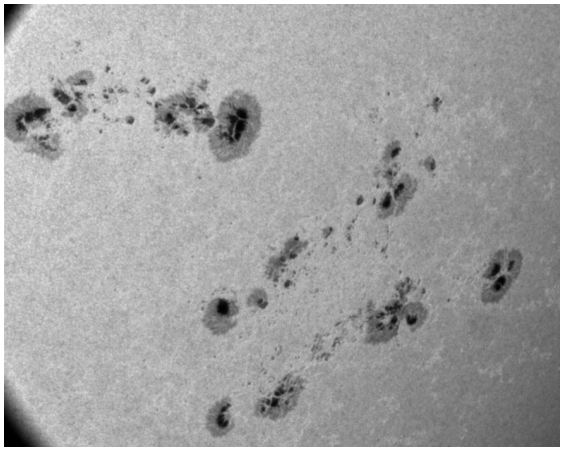

Figure 2.3: Sunspot clusters picture taken by *The Transition Region and Coronal Explorer* (TRACE). The telescope took images in a range of wavelengths from visible to far UV [1]. Image credit: TRACE

2.1.2 Solar Flares

Solar flares consist of energetic explosions in the low solar atmosphere. They come as a result of a restructuring of the magnetic field by itself to a lower energy state. The released energy is converted by flares into plasma heating and kinetic energy of charged particles. This conversion can occur through different mechanisms e.g. the reconnection of magnetic field lines (see section 2.2.3). Flares usually show two distinct phases : the initial impulsive phase and the subsequent transient gradual one. We are only interested in the impulsive phase because this is the period of the explosive release of energy. The gradual phase is long duration, rich in protons and associated with coronal and interplanetary shocks. Most of the flares take place in active regions - i.e. in the neighbourhood of sunspots where the solar magnetic field is highly concentrated - but smaller flares can occur at the boundaries of the quiet Sun. Flares emit radiation across the entire electromagnetic spectrum - from radio to γ-rays. These radiations may originate from different processes and not necessarily simultaneous or cospatial [5, 45]. Details about X-rays and γ-rays production will be developed in section 2.2.1 and further information about other radiations can be found in [5, 45].

A first classification of flares is realized according to the maximal intensity of the thermal flux measured by *GOES* in the X-ray band ($1 - 8$Å). It goes from A to X as following

A	=	1.0×10^{-8} W m^{-2}
B	=	1.0×10^{-7} W m^{-2}
C	=	1.0×10^{-6} W m^{-2}
M	=	1.0×10^{-5} W m^{-2}
X	=	1.0×10^{-4} W m^{-2}

A linear scale completes this classification by adding a number between 1 and 9 which represents the specific intensity of the flare. For example, a C5.9 flare means a flare of 5.9×10^{-6} W m^{-2}. Nevertheless some more energetic flares than a X9-flare have been detected such as the X28-flare which occurred on November 4th, 2003 during the 23^{rd} solar cycle. This classification indicates that solar flares may occur at many sizes : the largest have energies of 10^{33} erg or even 10^{34} erg for the most largest ones reported while the smallest in active regions have energies below 10^{26} erg. These estimations are

done considering the X-rays emission by non-thermal electrons with energies above 20 keV hitting a cold thick target (see Section 2.2.2) [9, 33, 5]. The reader will note that we have only considered the most energetic flares in this study (explanations in Section 4.3).

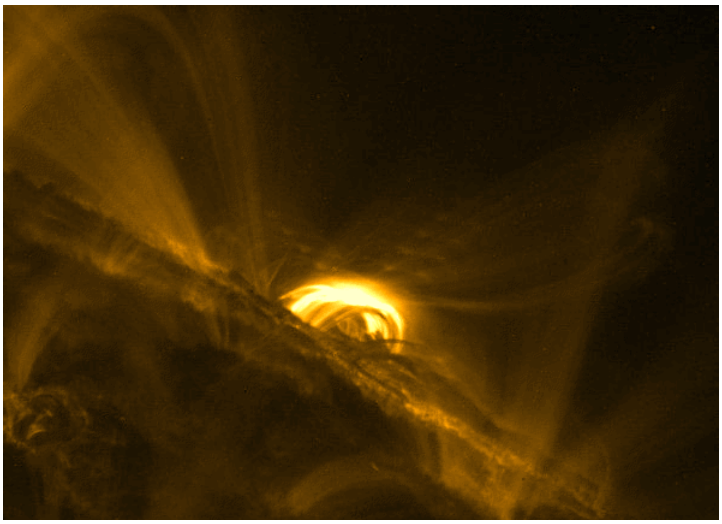

Figure 2.4: Hot flare loop imaged by the TRACE satellite [9]. Image credit: TRACE

2.2 X-rays, γ-rays and Neutrinos

Both X-rays and γ-rays have an important role in this study: the former are produced in electromagnetic processes while the latter may indicate either electromagnetic or hadronic acceleration. Neutrinos will only originate in hadronic processes and are thus important messengers to consider for resolving this ambiguity.

2.2.1 X-rays and γ-rays

Physics

X-rays are produced - through bremsstrahlung of accelerated electrons - in high density regions of the chromosphere and transition region. They are seen during the impulsive phase of a flare [5]. Due to their prompt emissions, they tag the start time of the solar flare in this study. .

As specified above, γ-rays are emitted due to the hadronic acceleration. They may be produced by nuclear deexcitation, neutron capture and positron annihilation. Some broad-band γ-rays extending to energies above 100 MeV are also observed as a result of pion decay. The neutral pions decay directly into two γ-rays; secondary positrons

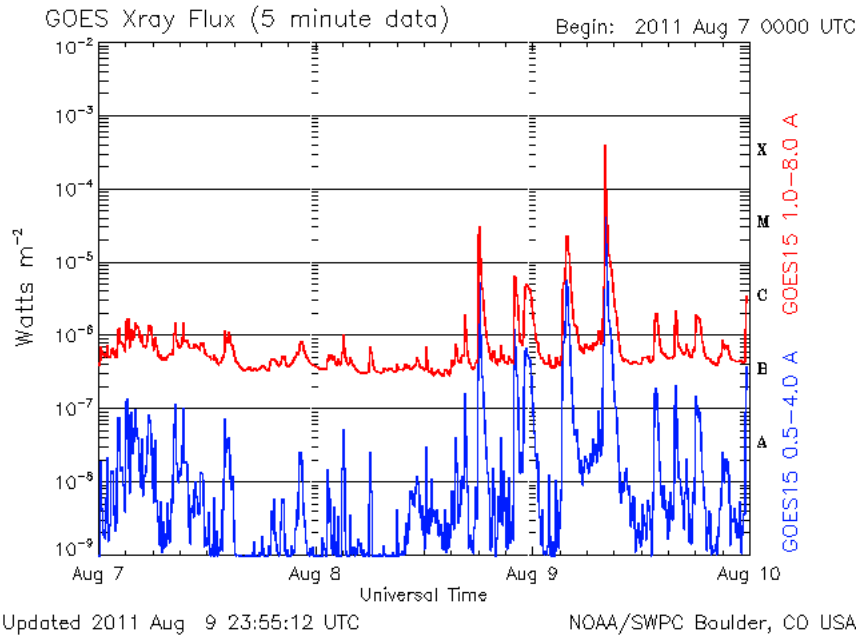

Figure 2.5: This plot contains 5 minute averages of solar X-ray output (W m^{-2}) in the 1-8 Angstrom (red) and 0.5-4.0 Angstrom (blue) passbands [64]. Data have been recorded by GOES15. [64]. The blue and red largest peaks in this plot indicate the X6.9 solar flare which occurred on August 9^{th} 2011. This flare is analysed in Chapter 5. Image credit: NOAA/SWPC

and electrons produced in charged pion decay emit these radiations by annihilation and bremsstrahlung [59]. Given their production channels, γ-rays may be highly delayed with respect to X-rays; they indeed can occur hours after the impulsive phase [30].

Detection

X-rays X-rays are detected by satellites such as the *Geostationary Operational Environmental Satellite* (GOES). Figure 2.5 shows some data recorded by GOES. The GOES satellites carry a Solar X-ray Imager to monitor the Sun's X-rays. They play an important role as X-ray detection is the earliest warning of solar flares, coronal mass ejections or other phenomena which impact the geospace environment [64]. The monitoring of these kind of events is essential to prevent harm to astronauts and military and commercial satellites.
To carry out the analysis, we will use GOES data as a time flag marking the flare's beginning (Section 4.4).

γ-rays The Fermi observatory was launched in 2008 to explore high-energy phenomena in the Universe. It comprised of two instruments [52, 58, 17]:

- the *Gamma-ray Burst Monitor* (GBM) designed to detect γ-rays from 8 keV up to 40 MeV. The Fermi GBM instrument consists of twelve NaI detectors pointing in various directions to measure the low-energy spectrum. Higher energy γ-rays are detected by two BGO detectors pointing in opposite directions.
- the *Large Area Telescope* (LAT) sensitive to γ-rays from 20 MeV up to more than 300 MeV. The LAT is a pair-conversion telescope with a precision tracker and calorimeter.

These data will be used as a time flag of the flare's end in our study.

2.2.2 Neutrinos

Physics

Neutrinos point out the hadronic acceleration. They are produced due to the charged pion decay as shown in Equations 2.1.

$$p_C = p\,(\text{from the chromosphere}) \qquad p_A = p\,(\text{accelerated}) \qquad (E_{p_A} \approx \text{GeV})$$

$$p_A + p_C \longrightarrow \begin{cases} \Delta^{++} + n \longrightarrow p + n + \pi^+ \\ \Delta^{+} + p \longrightarrow \begin{cases} p + p + \pi^0 \\ p + n + \pi^+ \end{cases} \end{cases} \tag{2.1}$$

$$\pi^+ \longrightarrow \mu^+ + \nu_\mu \qquad \mu^+ \longrightarrow e^+ + \nu_e + \bar{\nu}_\mu$$
$$\pi^0 \longrightarrow 2\gamma$$

Similar reactions may occur by proton-alpha scattering :

$$p + \alpha \longrightarrow \begin{cases} \Delta^{+} + n \longrightarrow n + n + \pi^+ \\ \Delta^{0} + p \longrightarrow \begin{cases} p + p + \pi^- \\ p + n + \pi^0 \end{cases} \end{cases} \qquad \pi^- \longrightarrow \mu^- + \bar{\nu}_\mu \qquad \mu^- \longrightarrow e^- + \bar{\nu}_e + \nu_\mu$$

Nevertheless these interactions have a lower probability than those in Equations 2.1 [22]. It may be shown that these interactions occur in the chromosphere. A lower limit on the ambient gas density can indeed be fixed by e.g. the slowing-down and annihilation time of the positrons. An upper limit is set by observations of neutrons escaping from the Sun. Another evidence - that the interaction region lies above the top of the photosphere - is the absence of the attenuation of low-energy γ-ray lines relative to higher-energy lines depending on the optical depth [59, 49].

These kinds of interactions may also occur in the Earth atmosphere and thus a second flux of neutrinos is produced. Nevertheless this flux has some clear differences with what we will call the *solar flux* i.e. the flux produced by interactions described in Equations 2.1. Besides being widely spread due to the curved trajectory of charged particles in solar and earth magnetic fields, this neutrino flux will be delayed by days with respect to the *solar flux*. This delay is due to the time it takes for relatively slow-moving proton clouds accelerated in solar flares to reach Earth. This later signal does not have a great physical interest [22, 23].

Detection

Neutrinos are detected by underground / under-ice detectors such as the *Homestake Chlorine Detector*, the *Kamiokande* (KAM-I and KAM-II), the *Sudbury Neutrino Observatory* (SNO) or *IceCube Neutrino Observatory*. These detectors have reported results about correlation between neutrino detection and solar flares. We therefore briefly describe those. IceCube is described in Chapter 3.

- The Homestake experiment - a 380 m^3 tank of perchloroethylene - was based on the inverse beta decay reaction

  $$\nu_e + {}^{37}Cl \rightarrow {}^{37}Ar + e^-$$

  Therefore, counting the number of argon that had been formed determined how many neutrinos had been captured. This experiment was designed to measure the total flux of solar neutrinos above 0.814 MeV. [27].

- Originally dedicated to search for nucleon decay, the Kamiokande was a water Cherenkov detector. It consisted of a 3,000 tons tank of pure water and an additional 1,500 tons of water using as a veto layer. It measured the energy, direction, and time of the recoil electron from elastic scattering of solar neutrinos with electrons by detection of the emitted Cherenkov light [51]. *Super-Kamiokande* - the current detector - and the future planned *Hyper-Kamiokande* constitute the next generations of this detector.

- SNO consists of an inner volume which contains 10^6 kg of heavy water. It has been constructed to study the fundamental properties of neutrinos, in particular the mass and mixing parameters. The heavy water permits detection of neutrinos through the neutral current and electron (anti-)neutrino charged current interactions and the elastic scattering [18, 19].

2.2.3 Acceleration mechanisms

The remaining question is how charged particles are accelerated. This section develops briefly acceleration mechanisms which could be involved in solar flares.

Acceleration of particles requires an electric field that could be in this framework:

- a large-scale externally imposed field
- a $(\bar{v} \times \bar{B})$ field
- a collective field associated with the environment in which the particle finds itself as for example a collisional Coulomb field

This variety of electric field sources involves a wide variety of possible acceleration mechanisms. Four mechanisms are briefly explained here but it is important to note that each combination of those can also be considered as relevant mechanisms. Here follows an intuitive description of the four main mechanisms which could be involved in the particle acceleration in solar flares. A complete description would require demonstrations using plasma physics equations which go far beyond the topic presented here. These mechanisms might take place above and in the chromosphere.

- **Reconnection models:** The electric field produced by magnetic reconnection[1] in solar flares is one of the most promising acceleration mechanism. It may occur when two magnetic tubes of opposite polarity merge forming a current sheet. The plasma will run in the middle and the magnetic field energy release is converted in plasma velocity. There is no privileged direction for accelerated particles: they can either escape along open field lines and be ejected in the interplanetary space or either go towards the dense chromosphere, interact with it and produce secondary particles as described in Section 2.2.2. The number of accelerated particles in this model is limited by the width of the current sheet. Several models of reconnection exist: some think that plasma effects increase the reconnection rate while other say that this increase is due to turbulence. See [69, 42, 11, 43, 36] for more information.
- **Shock acceleration - First order Fermi:** This mechanism is a demonstrated accelerator of charged particles in interplanetary space or in the Earth's atmosphere for example. It might also play a role in particle acceleration in solar flares. The general principle of Fermi acceleration is the energy transfer from macroscopic motion to microscopic particles. It happens through the interactions with magnetic homogeneities. The first order Fermi acceleration assumes that this macroscopic motion is coherent. Particles in solar flares can gain energy bouncing back a shock wave which could be a blast wave or slow shock occurring around the reconnection regions. More information in [47, 11, 61].
- **Magnetic trap: Betatron acceleration + First Fermi acceleration:** A collapsing magnetic trap located between the flare loop and the reconnection region might support the acceleration of charged particles. Two effects might be involved

[1] Reconnection cannot take place in regions where the "frozen-in" approximation is valid. In this approximation, plasma is frozen in to the magnetic field or in other words, plasma follows the magnetic lines. A break down in the ideal magnetohydrodynamics conditions is therefore necessary which means that diffusion regions are required.

in particle acceleration in this configuration: a decrease in the trap length - associated with the first order Fermi acceleration and called the mirror effect - and a contraction of the trap called the betatron acceleration. Details are developed in [63, 46, 11]. The region where the collapsing magnetic trap takes place is illustrated in Figure 2.6.

- **Diffusion models - Stochastic-Second order Fermi:** As already mentioned for the first order Fermi acceleration, particles can increase their speed by scattering off some magnetic irregularities. The second order Fermi acceleration - the version elaborated by Fermi himself - assumes that magnetic scattering centers have random velocities. The energetic gain is therefore fewer than the gain arisen from a first order Fermi acceleration. We do not derive the relation here but to give an idea the second order will lead to an energy gain of order $\frac{\Delta E}{E} \propto \beta^2$ while the energy gain in the first order Fermi scales as $\frac{\Delta E}{E} \propto \beta$ where β is the average velocity of scattering center in units of the speed of light. Further information in [69, 47, 11].

The aim of this section was to give an idea of the variety of acceleration mechanisms proposed by theory. Each model has advantages and failings which reflects the difficulty of flare modeling. There is indeed no flare model yet [5].

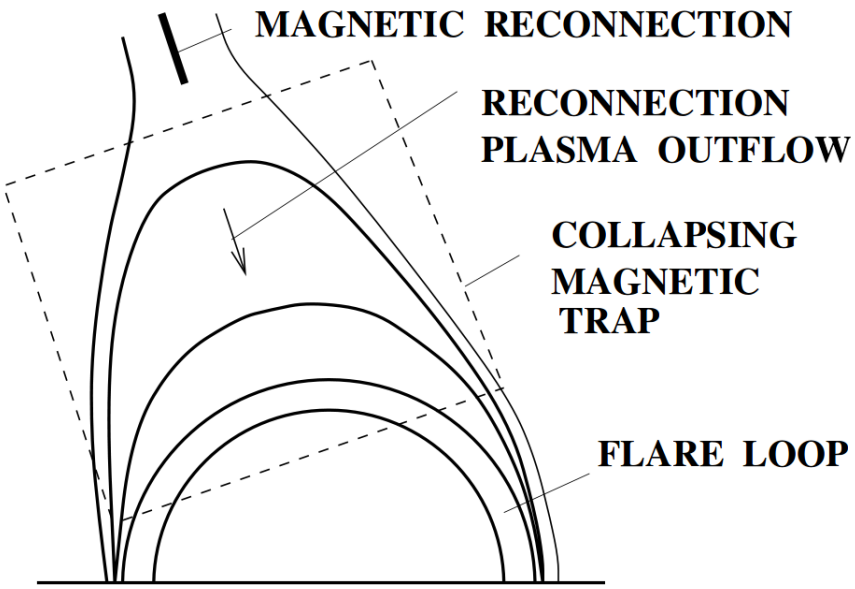

Figure 2.6: Illustration of possible magnetic configuration of a solar flare [46].

2.3 Neutrinos and Solar Flares - state of the art and interest

2.3.1 State of the art

Davis et al. have reported an excess in the neutrino-capture rates in the chlorine detector. Associating the excess events with solar flares, Davis estimated 20-250 excess neutrino captures per flare corresponding to the times of occurrence of the solar flares in his detector [38].

Hirata et al. indicated that no significant neutrino signal was found at the time of a solar flare in the period between 1983 and 1988 in the Kamiokande detector. They concluded that the data of their detector do not support the hypothesis of an increase in neutrino flux at energies $E_\nu \geqslant 50MeV$. However, these data correspond to a period near the minimum of the 11-year solar-cycle. Therefore, they added that it remains interesting to seek an increase in neutrino flux in coincidence with a strong flare or during periods of maximum solar activity [38].

More recently, the Sudbury Neutrino Observatory collaboration published its results about a search for neutrinos associated with sources other than the solar core. Concerning solar flares, they concluded that their analysis excludes the Homestake results down to approximatively 2.2 MeV. They assumed that all the neutrinos are generated as ν_e in the Sun's atmosphere and then oscillate with a probability to stay in the electronic flavor of 0.55 [19].

A significant difference between these results and those of Kamiokande or Homestake is that the former are obtained from multiple bursts while the latter came from a single flare. The integration time that has been considered is also considerably different : the Homestake run lasted 6 days while the SNO results are obtained with a shorter time corresponding to the actual flare [19]. A comparison of results obtained by the different collaborations can be seen in Figure 2.7.

Section 3.4 describes the main differences between these studies and the one we carried out.

2.3.2 Relevance of neutrinos in the study of solar flares

There is more than one interest to study neutrinos coming from solar flares. The most obvious one is that they constitute an unique insight in hadron acceleration. Unlike γ-rays, neutrinos are only produced by accelerated hadrons. Therefore, studying the delay between X-rays, γ-rays and neutrinos should provide information about the difference between lepton and hadron acceleration [59].

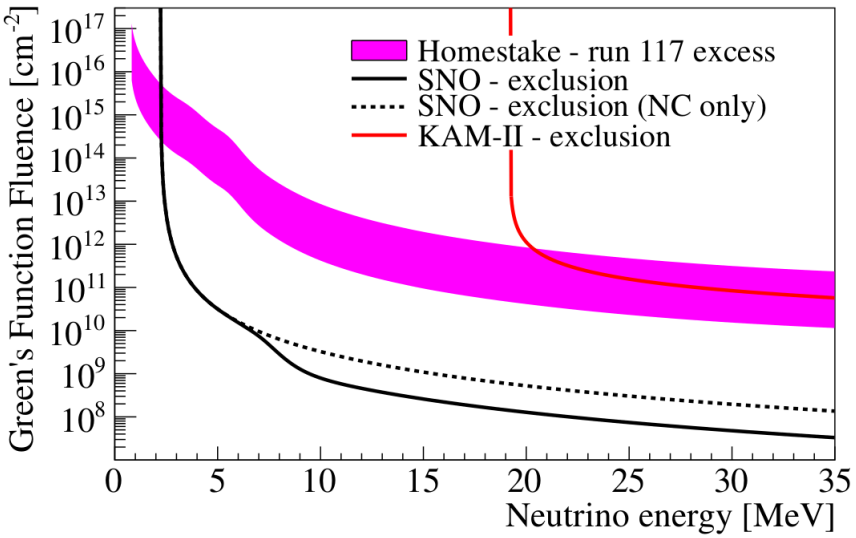

Figure 2.7: This plot shows the solar flare neutrinos fluence versus neutrino energy. The results for all experiments are calculated assuming pure ν_e production in the solar atmosphere and include vacuum oscillations during their journey to Earth [19]. Image Credit: SNO collaboration

Chapter 3

IceCube

This study is conducted using IceCube, the neutrino telescope buried in the South Pole ice. This chapter firstly describes interactions of neutrinos with matter in the following section and the benefit of using large amounts of ice or water to detect them in section 3.2. A brief technical description of the detector is presented in section 3.3. Section 3.4 describes the main differences between the study we carried out and previous solar flare studies.

3.1 Neutrino interactions with matter

As mentionned in Section 1.2, neutrinos interact only through the weak force. This section describes the interactions of neutrino with ordinary matter: nuclei and electrons. There are different kinds of interactions and each one can be highlighted by the signature of the particles which have been produced in the detector.

- One of these possibilities is the NC interaction : a neutrino interacts with a nucleus through the exchange of a Z boson. In this interaction, the neutrino scatters a quark q of a nucleus and produces a hadronic shower X as shown in Equation 3.1 and Figure 3.1(a).

$$\nu_l(\bar{\nu}_l) + q \rightarrow \nu_l(\bar{\nu}_l) + X \tag{3.1}$$

- A second possibility is the exchange of a W boson through a CC interaction. The neutrino interacts with a quark q of a nucleus to produce a charged lepton $l^{\pm}$ and a hadronic shower X as shown in Equation 3.2 and Figure 3.1(b). It is important to note that the charged particle produced in this interaction belongs to the same generation as the neutrino.

$$\nu_l(\bar{\nu}_l) + q \rightarrow l^-(l^+) + X \tag{3.2}$$

In each signature of neutrino interactions with matter presented in Figure 3.2, a hadronic cascade is produced at the interaction point [66]. In the case of CC interactions presented

in Figures 3.2(b), 3.2(c) and 3.2(d) a charged lepton is also produced at the interaction point. Each charged lepton has a different signature in IceCube and thus some level of flavour identification can be realised. Electrons will produce an EM shower or cascade, while muons, heavier than electrons will pass through the ice in a nearly straight manner[1]. The 0.29 ps mean lifetime of the tau lepton implies that it will decay after a short path in matter and will produce a secondary shower or a μ in about 17% of the time [66, 67].

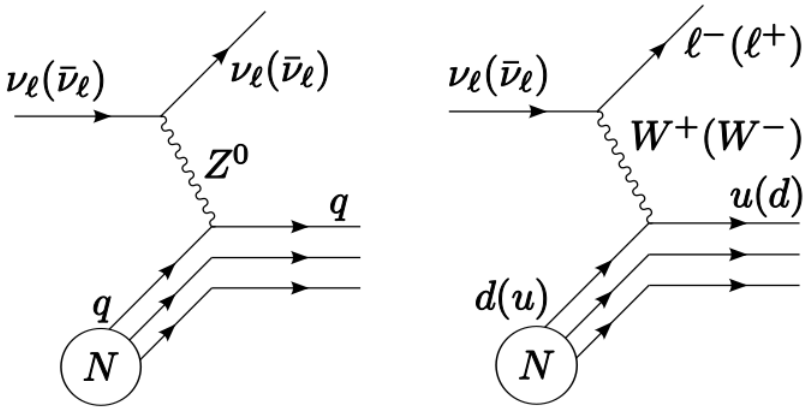

(a) NC interaction (b) CC interaction

Figure 3.1: NC and CC interactions between neutrino and quarks. The CC interaction turns a d (u) quark to a u (d) quark meanwhile the ν is turned to its associated charged lepton.
[66].

At GeV scale, the neutrino-electron scattering, Equation 3.3, may be neglected as shown in Figure 3.3. The charged and neutral current cross sections are indeed more than 100 times smaller than the corresponding nuclear interactions in Equations 3.1 and 3.2.

$$\nu_l + e^- \rightarrow \nu_l + e^- \tag{3.3}$$

Illustrations of charged lepton signatures in the IceCube detector are presented in Section 3.3.1.

[1]Given that the bremsstrahlung cross section is $\propto \frac{1}{m^2}$ where m stands for the mass of the charged particle. See also Section 3.4

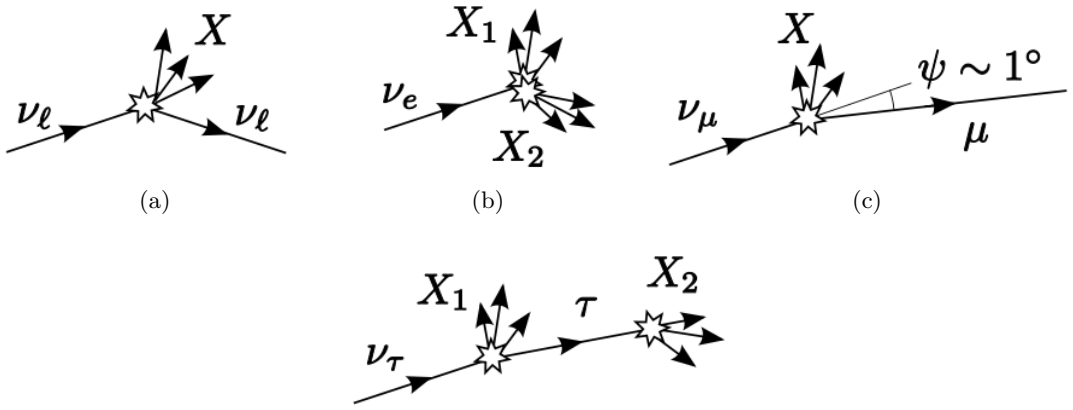

(a) (b) (c)

(d)

Figure 3.2: Signatures of NC and CC interactions between neutrino and nucleus. NC interaction of neutrino is illustrated in Figure a). The neutrino scatters off a nucleus leaving no other visible signature than the hadronic cascade. The hadronic cascade typically carries 20% of the initial neutrino energy. Figure b) shows the interaction of an electron neutrino with matter: it produces an electromagnetic shower. In Figure c) a muon neutrino interacts and a long ranging muon is produced on a direction close to the neutrino direction. The tau neutrino interaction is shown in Figure d): a short range lepton tau is created. When the tau decays a secondary shower is produced. This double shower signature can be used to identify tau events. These three last interactions are CC interactions [66].

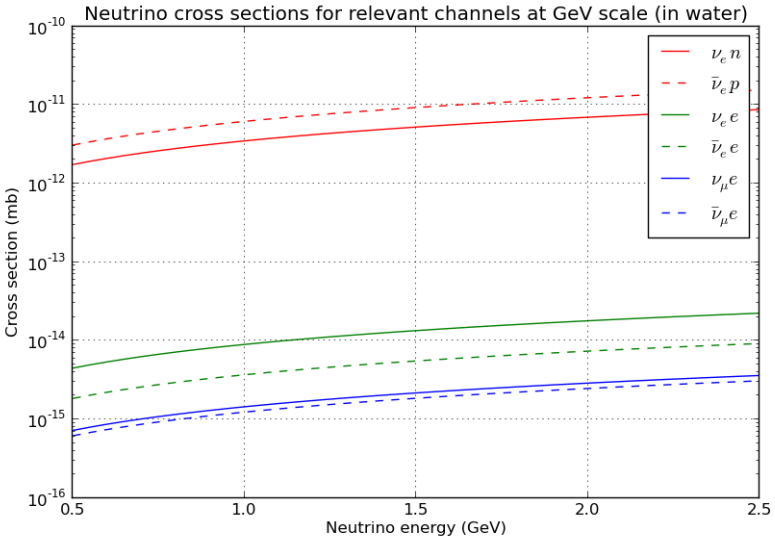

Figure 3.3: Neutrino cross sections for relevant channels at GeV scale. The different colors stand for the different channels. Cross sections have been taken in [22].

3.2 Detecting neutrinos

In 1960, M Markov published his groundbreaking idea to detect high energy muon neutrino:

"... we propose to install detectors deep in lake or a sea and to determine the direction of charged particles with the help of Cherenkov radiation"

This proposition marks the beginning of the era of neutrino detection through underground detectors using the Cherenkov radiation. It contained already all relevant characteristics of neutrino detectors [31, 32] :

- *deep* in order to use the Earth as a shield against atmospheric particles (see section 3.2.1).
- *in lake or a sea* to have a detection volume large enough to collect neutrinos in statistically significant numbers. Markov thought only about liquid water as the detection medium. However, there is no constraint on the medium that can be used, except that its refraction index must allow the production of a Cherenkov radiation for high energy particles. The medium has also to be transparent to this radiation (see section 3.2.3).
- *cherenkov radiation* to, due to the light cone emitted, detect the charged particle emitted in the CC-interaction between neutrino and the medium (see section 3.2.2).

3.2.1 The Earth as a shield

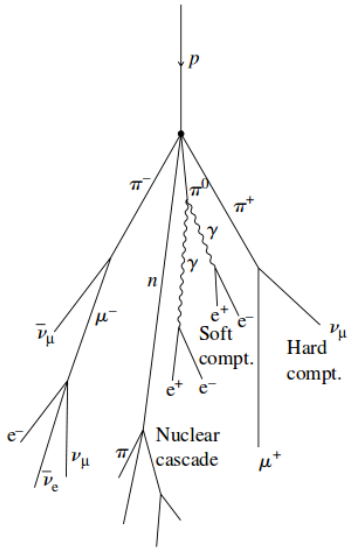

Figure 3.4: Hadronic shower [55]

The background Atmospheric μ and ν_μ are by far the most numerous events recorded by IceCube. Atmospheric μ constitute indeed more than 99% of the signal. These particles are produced in cosmic ray showers. These showers are initiated by accelerated hadrons travelling in the Universe. When these particles reach the Earth and collide with nuclei of the atmosphere, an hadronic shower, shown in Figure 3.4, is created. These events constitute the background of IceCube analyses. The Earth is used as a shield against atmospheric μ since their range is not sufficient to reach the detector after crossing the Earth (see section 3.4). Atmospheric neutrinos constitute an irreducible background since they can cross the Earth without being stopped.

The MeV neutrinos coming from nuclear reactions taking place in the center of the Sun will not represent a background for our study. IceCube has indeed a detection threshold above the MeV scale [37].

3.2.2 Cherenkov radiation

When a charged particle traverses a medium with a velocity higher than the speed of light in this medium it loses energy in the form of a coherent wavefront of Cherenkov radiation. The emitted light is mostly in the UV and blue region of the electromagnetic spectrum. The Figure 3.5 shows the Huygens construction for this effect. It comes

$$\cos\theta = \frac{(ct/n)}{\beta ct} = \frac{1}{\beta n} \qquad \text{with the condition : } \beta > \frac{1}{n} \tag{3.4}$$

where

- n stands for the refractive index of the medium
- c represents the speed of light in vacuum
- t is the time
- $\beta = \frac{v}{c}$ for a particle with a velocity v

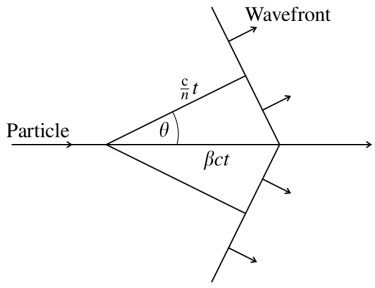

Figure 3.5: Huygens construction [55]

The amount of light generated through the Cherenkov effect is

$$\frac{dN^2}{dEdx} \approx 370 \sin^2\theta(E) \text{ eV}^{-1}\text{cm}^{-1}$$

This Cherenkov light will allow the detection of charged particle (see section 3.8) [66, 55, 37].

3.2.3 Propagation of light in the South Pole ice

Ice has a capital role in IceCube since it is used as a Cherenkov radiator. Knowledge of the properties of the ice surrounding the detector is therefore essential to evaluate the optical absorption and the scattering of Cherenkov photons i.e. to determine what IceCube observes. Impurities and air bubbles indeed strongly influence the optical transmission. Figure 3.6 shows the scattering and absorption lengths as a function of depth and wavelength. The impact of air bubbles and the presence of a dust layer are highlighted by an increase in scattering and absorption lengths. With the exception of those regions, the South Pole has an extremely clear ice and therefore allows a photon propagation over long distances.

The current ice model used by IceCube is *SPICE-MIE*, a direct fit approach to fitting the ice properties [14, 32, 50]. This model has been used in our Monte Carlo simulations (see section 4.1).

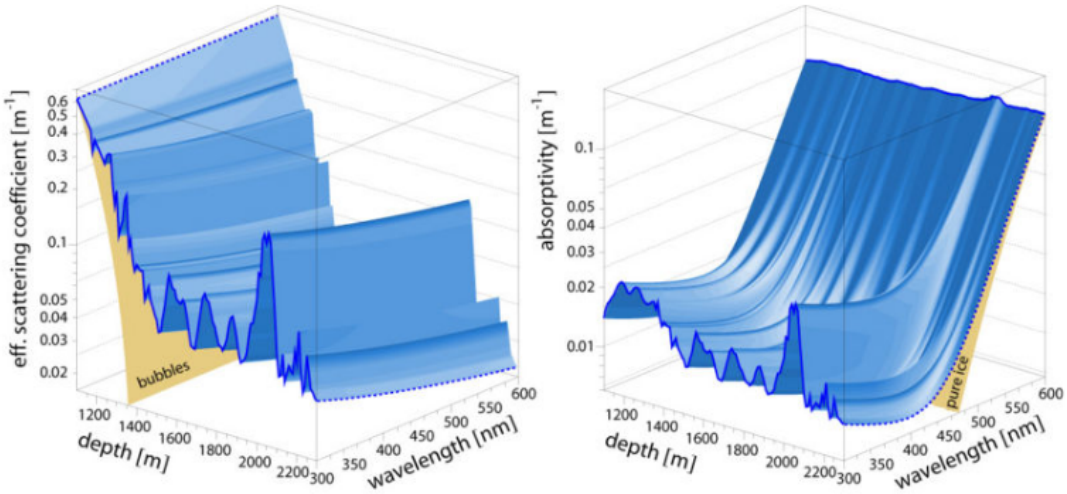

Figure 3.6: Scattering and absorption lengths of light in South Pole ice as a function of depth and wavelength. These curves are based on theoretical models and IceCube measurements [14, 32].

3.3 IceCube detector

The fascinating story of the birth of IceCube told by F Halzen can be read in [8].

Completed since 2011, IceCube contains 86 vertical strings[2] each containing 60 *Digital Optical Modules* (DOMs) (see section 3.8). It is a $1km^3$ volume located between 1450 and 2450 meters below the surface of the South Pole. Figure 3.7 shows the IceCube layout. The typical distance between two strings is about 125 m while each DOMs is separated by about 17 m from its neighbour along each string.

IceCube was optimised for the detection of TeV-scale neutrinos of astrophysical origin, some 2-3 orders of magnitude more energetic than the GeV neutrinos expected from solar flare events. However, the IceCube DeepCore sub detector array was installed to extend the physics capabilities of IceCube to lower energies by providing a denser deployment of optical instrumentation in the clear, deep ice. Six additional strings situated on a denser 72 m hexagonal grid have been added. DeepCore DOMs are located every 7 m and have a higher quantum efficiency than standard IceCube DOMs. Two of the IceCube strings have the standard DOMs but 7 m vertical spacing and even smaller horizontal spacing of 42 m. These 8 strings and the 12 surrounding IceCube strings form DeepCore. DeepCore is distributed around the dust layer as shown in Figure 3.7.

A surface array dedicated to air shower studies - IceTop - is also included in the detector. It consists of 160 tanks, placed by pair at the top of each string. In addition to studying the composition and spectrum of cosmic rays (CR), IceTop can be used as a atmospheric μ veto for IceCube analyses [44, 32, 37].

3.3.1 Illustrations of typical IceCube events

Figures 3.9(a) and 3.9(b) show typical signatures that muons and electrons respectively leave in IceCube. DOMs colors are a time indication : earlier the DOM has been hit by Cherenkov photons, redder it is. The tau signature has not yet been observed in IceCube.
Events presented in Figure 3.9 have a much higher energy than 1 GeV. Therefore solar flare neutrinos will not able to produce charged leptons having this kind of signature (see sections 3.4 and 4.2).

3.3.2 Digital Optical Module

Digital Optical Module, data acquisition and calibration sections are highly inspired by [44].

The *Digital Optical Modules* (DOMs) constitute the fundamental detection element in IceCube. The Figure 3.10 shows all the components of a DOM and the Figure 3.8 is a picture of a DOM. Each DOM contains a 25 cm diameter Hamamatsu R7081-02 *Photomultiplier Tubes* (PMT) to detect blue and near-ultraviolet Cherenkov light.

[2] We will call IceCube with 86 strings IC-86

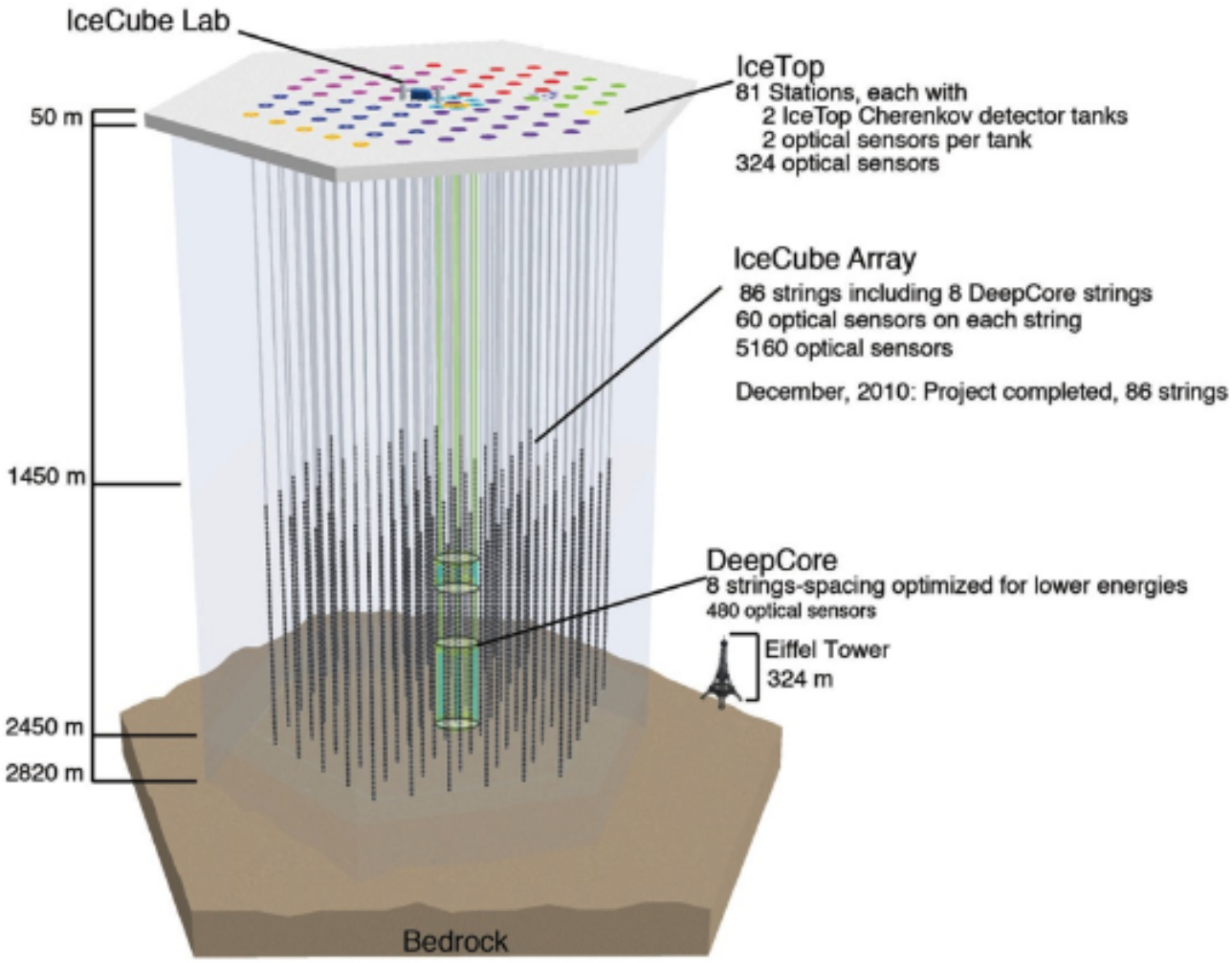

Figure 3.7: Schematic representation of the IceCube detector [37].

It has a rate of 500 Hz in the dark and at -40°C. The signal transit time spread is 3.2μs. To run the PMT at a gain of about 10^7, a 2 kV high voltage DC/DC power supply is used. It provides a bias voltage of between 1200 V and 1400 V to the PMTs. Each DOM has a main board which is responsible for processing the analog output of the PMT. Given the high pressure exerted during the deployment, each DOM has a 13 mm thick glass sphere; a gel between this glass and the PMT provides support and optical coupling. A DOM includes also a flasher board which contains twelve light emitting diodes (LEDs). The role of this flasher boards consists of performing *in situ* calibrations such as timing, geometry, energy and measurements of the optical properties of the ice. Finally, a mu-metal cage shielding the Earth's magnetic field ensures that electrons produced by a photon in the photocathode travel directly to the anode [44].

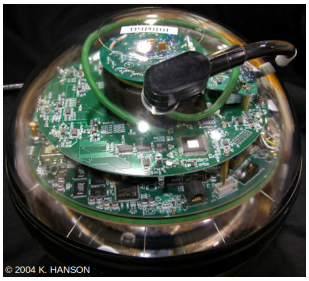

Figure 3.8: A DOM [37]

3.3.3 Data acquisition

The first goal of the *IceCube Data Acquisition* (DAQ) is to capture and timestamp the optical signals with the maximum possible dynamic range and with a high time precision. A single Cherenkov photon arriving at a DOM can produce a photoelectron. The DOM will be considered as *hit* if the analog output of the PMT exceeds a threshold equivalent to ~ 0.25 of the average single photoelectron charge. The waveform of the PMT total charge is digitized and sent to the surface if there is a local coincidence. It means that hits have to be in coincidence with at least one other hit in the the nearest or next-to-nearest neighbouring DOMs within $\pm$1000 ns. There are two waveform digitization systems : the analog transient waveform digitizer (ATWD) and the fADC (fast ADC) Details about the digitization of the signal can be found in [44, 32]. All DOMs run power and communications through a single 44 mm dia. cable of twisted-wire pairs. The cable runs to the surface and is connected to a central counting house in the IceCube Lab (see Figure 3.7). A simple multiplicity trigger which requires local coincidence hits in eight DOMs within 5 μs is used. This trigger is called SMT8 [44]. Considering the low energy expected for solar flare neutrinos, a lower trigger condition than SMT8 - the SMT3 - has been used as in many DeepCore analyses. This trigger condition requires three or more hit DOMs - in the DeepCore or the nearest neighbourhood - satisfying the *Hard Local Coincidence*[3] (HLC) condition within a 2.5 μs time window [15].

3.3.4 Calibration

The timestamp of hits of each DOMs is done by a 20 MHz crystal oscillator with a certified stability of $\sim 10^{-11}$ over 5 s. The *reciprocal active pulsing calibration* (RAPcal) is performed in order to keep all DOMs clock synchronized and each DOMs receive a precisely timed pulse from a central GPS clock. Each DOM receives this RAPcal signal

[3] At least two hit DOMs in the nearest neighbourhood in a time window of $\pm 1 \mu s$ (see [13] for more informations)

and records the arrival time according to its local clock. The DOM generates a nearly-identical response and transmits to the surface. The reciprocal symmetry between the oppositely-traveling signals ensures an equal transit time (down to small variations in electronic components). By accounting for transit times and the RAPcal timestamp from the DOM, a single GPS clock is used to transform the hit times to a global time.

A gain calibration is also needed. It is automatically performed once per year. It has to ensure that each DOMs are operating at the proper voltage to achieve the 10^7 gain.

More details about calibration but also triggering, filtering and reconstruction can be found in [32].

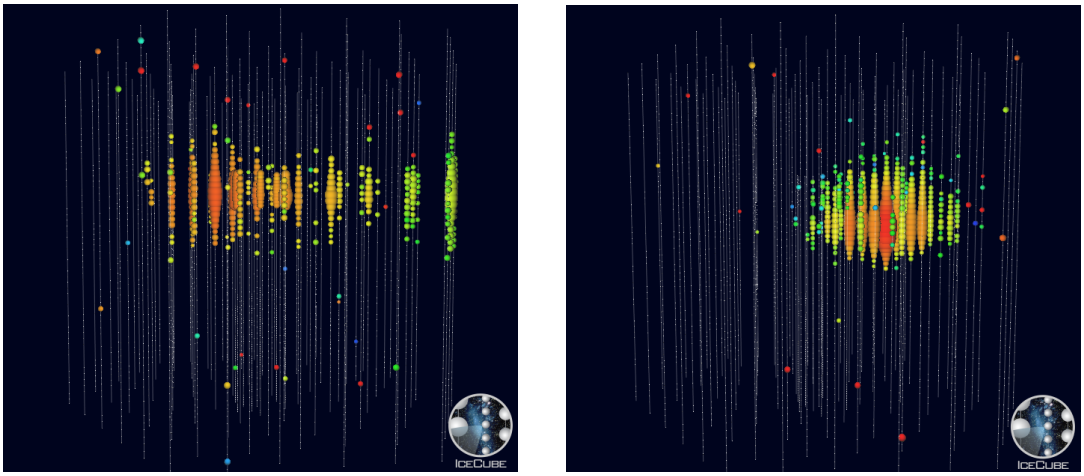

(a) (b)

Figure 3.9: Typical signatures of a muon 3.9(a) and an electron 3.9(b) in IceCube

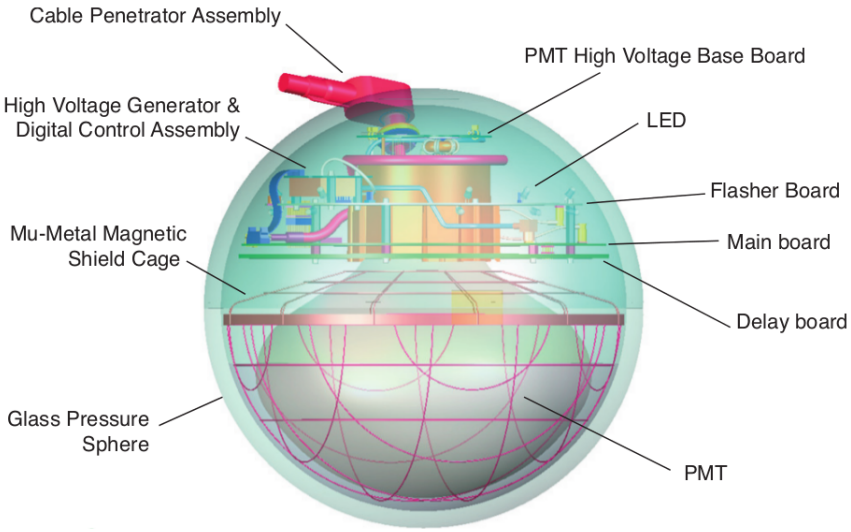

Figure 3.10: Digital Optical Module

3.4 IceCube as a solar flare neutrino detector

DeepCore analysis versus previous solar flare studies A main difference between the study we have carried out and the previous searches for solar flare neutrinos is the energy range which has been studied. All previous analyses were indeed searching for MeV neutrinos while our analysis is carried out at a GeV scale. Neutrino energy in GeV scale allows the production of muons through CC interactions between neutrinos and ice nuclei.

Unfortunately signatures of muon and electron are not different at GeV scale. The muon is indeed identified (see Sections 3.1 and 3.3.1) because of the track left in the detector but the GeV muon track is too short to be resolved.
Although crucial for the detection, the average energy loss due to Cherenkov radiation does not dominate for muons in ice. The four dominant processes are indeed :

- Ionization : this contribution is nearly energy independent at GeV scale (see the Bethe-Bloch formula).

- Bremsstrahlung
- e^+e^- pair production
- Photo-nuclear interaction

} energy dependent contributions

Considering the average rate of muon energy loss

$$-\frac{dE}{dx} = a(E) + b(E)E \tag{3.5}$$

where

- $a(E)$, the ionization energy loss, is given by $a \approx 0.26\,GeV\,\text{mwe}^{-1}$
- $b(E)$ - the sum of stochastic contributions - is $b \approx 3.6\,10^{-4}\text{mwe}^{-1}$

The energy of the muon E_μ can be determined when the stochastic contribution dominates i.e. when E_μ is above a treshold energy of $E_{th} = \frac{a}{b}$. The integration of Equation 3.5 leads to the mean muon range R_μ

$$R_\mu \approx \frac{1}{b} \ln\left(\frac{E_\mu}{E_{th}} + 1\right)$$

It means that the range for a GeV muon will be less than 5 meters; a reconstruction of the track is therefore not possible [28, 50, 67].

Chapter 4

Analysis

This analysis is divided in several parts which are explained here. The first part consists in a MonteCarlo simulation in order to evaluate the sensitivity of the DeepCore. A second step is to find a set of parameters to filter the entire set of IceCube data. After explaining how the final set of cuts has been chosen in Section 4.2 , we explain how we chose the solar flares in Section 4.3. Section 4.4 finally explains how data have been compared to solar flares.

It is important to note that this analysis substantially differs from usual analyses conducted by the IceCube collaboration. We will not be able to tag solar flare neutrinos events but we will monitor the number of this kind of events during solar flares.

4.1 Monte Carlo Simulations

A simple Monte Carlo simulation

A Monte Carlo simulation has been performed in order to determine the efficiency of the IceCube detector to hard, low-energy neutrino spectral distributions anticipated from solar flare acceleration mechanisms. This leads to determine the energy range of solar flare neutrinos which provokes the highest number of cascades per neutrino in our detector.
This simulation was a simple python code. A generic E^{-1} power spectral index of neutrinos [22] was assumed and the ice model used was a homogeneous bulk ice with an absorption length of 75 meters. Finally, the detector trigger condition - at least 3 hits recorded in the detector - was applied. This simulation led to evaluate the effective volume of the DeepCore according to

$$V_{eff} = \frac{N_{trig}}{N_{gen}} V_{gen}$$

where

- V_{gen} represents the generated volume i.e. $20\,10^6\,m^3$
- N_{gen} stands for the number of generated events
- N_{trig} which is the output of the simulation represents the number of events seen by the detector

Then the number of cascades per neutrino is given by

$$\boxed{N_{casc,\nu} = \rho\, N_A\, \sigma\, V_{eff}\, \phi}$$

where

- ρ is the density of the ice
- N_A represents the Avogadro number
- σ stands for the cross section between the neutrino and nuclei given by

$$\begin{cases} \sigma_{\bar{\nu}_e p} = 6.2\,10^{-39}\,\mathrm{cm}^2\,\left(\frac{\bar{E}_{\bar{\nu}_e}}{\mathrm{GeV}}\right) \\ \sigma_{\nu_e n} = 3.5\,10^{-39}\,\mathrm{cm}^2\,\left(\frac{\bar{E}_{\nu_e}}{\mathrm{GeV}}\right) \end{cases}$$

  These approximations are valid in the energy window we will consider i.e. $E_{\nu_e}, E_{\bar{\nu}_e}, E_{\nu_\mu}, E_{\bar{\nu}_\mu} \simeq 100 - 1000\,\mathrm{MeV}$ [22].
  Interactions with electrons may be neglected given the small charged and neutral current cross sections $\left(\sigma_{e\nu} \simeq 10^{-45}\left(\frac{\bar{E}_\nu}{\mathrm{MeV}}\right) cm^2\right)$.

- $\phi = A\,E^{-1}$ as already precised.

Figure 4.1 shows the number of cascades per neutrino from a solar flare event produced in the detector simulation, plotted as a function of the neutrino energy. Therefore the highest sensitivity of the DeepCore should occur for neutrino energies between 1 and 1.5 GeV.
Considering this and using the number of expected neutrinos from solar flares at sea level derived by D. Fargion[1] [22], we expect to find more than 870 cascades produced in the detector in a large flare ($E_{fl} = 10^{33}\,\mathrm{erg}$). This number must be placed in comparison with the IceCube DeepCore background integrated over the time window considered, 1500s around the flaring event. Our calculations indicate that this number fluctuates around 7500 hits the detector. It therefore follows that the number of expected cascades produced by a single large flare is larger than that required for a 3σ detection.

[1]The large number of models of particle production in solar flares reflects the uncertainty of physical phenomena that take place in these eruptions. The number of produced neutrinos will moreover depend on the solar region where the flare occurs: we intuitively expect more neutrinos from limb flares rather than central flares. The derivation considered here is the most optimistic one.

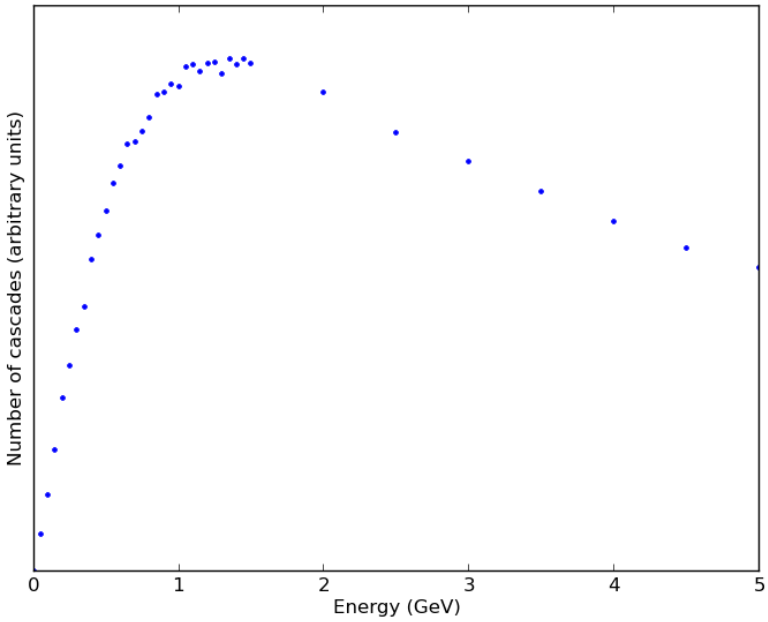

Figure 4.1: Number of cascades produced in the detector by a neutrino emitted during a solar flare. It shows that the DeepCore sensitivity should be maximal around $1-1.5\,\mathrm{GeV}$

CLSim Monte Carlo

A more developed Monte Carlo simulation has also been carried out. This simulation generated events in IceCube using GEANT4. The same generic flux as the one describe in Section 4.1 has been assumed. Only charged-current interactions for ν_e and ν_μ have been simulated although neutral current interactions occur for the three neutrino flavour; we have therefore fixed a lower limit on the effective mass expected. Randomly electromagnetic cascades have been generated using a Graphics Processing Unit. According to a known ice model, SpiceMie (see Section 3.2.3), the photon detections in the DeepCore optical channels were sampled. This sophisticated simulation is the simulation usually used by IceCube for the analyses. It essentially simulates the detector and all of the filtering cuts used in the data analysis. These files should only contain events arisen from solar flares.

Figure 4.2 shows the effective volume calculation for the CLSim and the simple Monte Carlo. The reader will note that the simple Monte Carlo is within 10 times the sophisticated simulation.

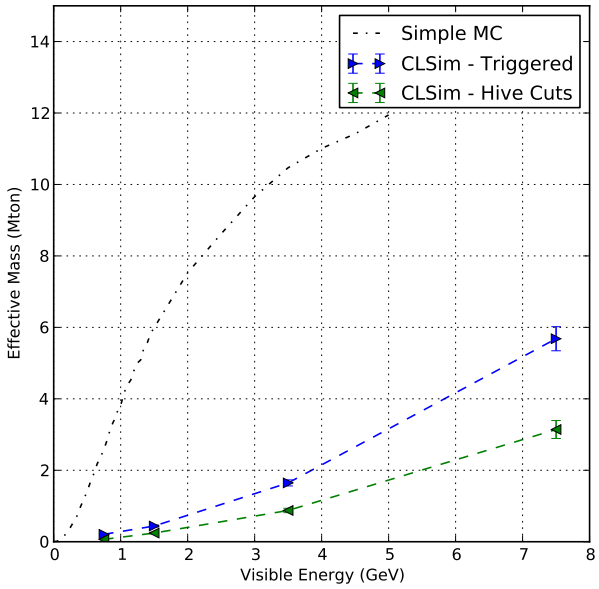

Figure 4.2: Effective volume obtained for the different Monte Carlo simulations. The simple Monte Carlo simulation are represented by grey dashed lines. Green and blue dashed lines stand for CLsim Monte Carlo : the green curve represents simulation after filtering process (see Section 4.2) while the blue one represents the entire simulation .

4.2 Cuts' development

The second step of this study was to find some parameters that can be used to select events which could arise from a solar flare. We assume that solar flare neutrinos trigger the detector. The DeepCore uses a SMT3 trigger : it requires three or more hit DOMs - in the DeepCore or the nearest neighbourhood - satisfying the *Hard Local Coincidence*[2] (HLC) condition within a 2.5 μs time window [15]. This assumption will have an impact on the choice of solar flares (see section 4.3).

First of all, it is important to understand which kind of signature solar flare neutrinos should produce in the detector.
As already explained, the DeepCore consists of some of the IceCube strings dedicated to study low energy events. Therefore selecting events which contain hit doms in this region was the first step of filtering. It has been easily done using the key parameter *FilterMask* of the IceCube software and by requiring that *DeepCoreFilter_11* is passed.

[2]At least two hit DOMs in the nearest neighbourhood in a time window of $\pm 1\,\mu$s (see [13] for more information)

The set of remaining events can be divided in three different groups:

"Muon-like events" Figure 4.3(c) represents what we will call a muon-like event. It typically comes from an atmospheric muon. It is important to realize that atmospheric muons constitute 99.999% of the signal in IceCube. These events constitute the background of this study.

"Solar-flare-like events"... or what it should look like Given the DeepCore sensitivity to solar flare neutrinos (see Section 4.1), GeV neutrinos should constitute the biggest part of our signal. Therefore, only few "causally connected" DOMs are expected. Since the speed of light limits the separation of physically related DOM hits, we can define causality relationship between hit DOMs. Two DOMs which may have been touched by the same cherenkov cone will be say "causally connected". Figure 4.3(b) shows what a solar-flare-like event should look like.

Noise events Figure 4.3(a) represents a typical random noise event. These events do not correspond to a physical event. It will be important to remove these events of the data because of their similarities with solar-flare-like events.

The filtering process will have to get rid of muon-like events but also of noise events. The former will be suppressed using a selection parameter described below while the latter will be identified using the NoiseEngine algorithm.

NoiseEngine cleaning The NoiseEngine algorithm was used to identify noise events. This algorithm is able to tag events as *most probably a random noise event* or *most probably a physics event*. A selection of the events tagged as *most probably a physics event* led to a strong suppression of noise events.

Selection parameters Several selection parameters have been tested to extract solar-flare-like events from the entire set of data. In order to check if the parameter distinguishes solar-flare-like events from muon-like events, the data were compared with a *COsmic Ray SImulation for KAscade* (Corsika) developed by the Kascade group [57]. This simulation can be used to create atmospheric muons' signature in IceCube.
Given the expected low energy of solar flare neutrinos, Corsika has to simulate a lot of low energy muons to make certain that the selection parameter gets rid of them. It means that an unweighted simulation had to be preferred. Therefore the CORSIKA-in-ice poly-gonato model with unweighted spectrum of Hoerandel using SPICEMie Photon Propagation Code, an angular range of $0\,\text{deg} < \theta < 89.99\,\text{deg}$ and energy range of $600\,\text{GeV} < E_{prim} < 1 \times 10^{11}\text{GeV}$ seemed to be the most appropriate simulation in this case [3].

[3] If the direction is expressed in a standard polar coordinate system with the z-axis pointing up, θ is the polar angle with respect to the z-axis

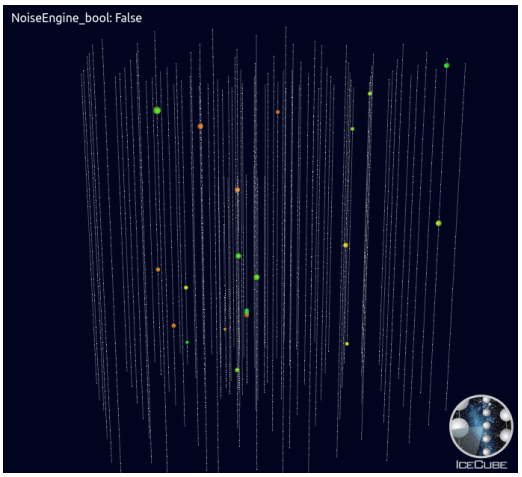

(a)

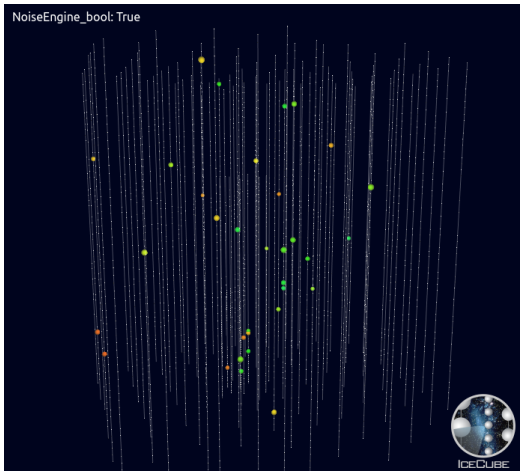

(b)

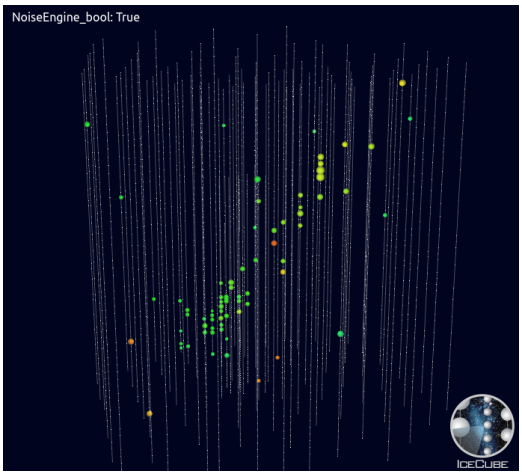

(c)

Figure 4.3: As it can be seen there is no visible difference between a noise event 4.3(a) and an event which could arise from a solar flare 4.3(b). Therefore the output of NoiseEngine will be useful: it will return *TRUE* if the event is *most probably a physical event* and *FALSE* if it is *most probably a random noise event*. A muon-like event, illustrated in 4.3(c), shows a radically different shape.

Details about poly-gonato model and spectrum of Hoerandel can be found in [40] while SPICEMie and the Photon Propagation Code are detailed in [34]. Plots related to the chosen parameter will follow while others can be found in Appendix 4.2.

Cut Parameters

The chosen parameter is connected to the causality of DOMs. The *TWSRTOfflinePulses* key is a parameter which select a set of DOMs which are causally connected to some seed-hits. These seed-hits are some kind of defined mostly-signal-like events as for example a HLC [37]. The *TWSRTOfflinePulses* DOMs are illustrated for each kind of events in Figure 4.5.

If N_T is the total number of hit DOMs and N_{cc} stands for the number of causally connected DOMs determined by the *TWSRTOfflinePulses* key, the chosen parameter, called RATIO, is defined such as

$$\text{RATIO} = \frac{N_T - N_{CC}}{N_T}$$

In other words this parameter evaluates, for each event, the ratio between the number of non-causally connected DOMs and the total number of hit DOMs. The comparison of data and Corsika with respect to this parameter is illustrated in Figure 4.4.
A clear difference between data and Corsika can be observed. Therefore, using a value of this parameter as a cut's threshold will distinguish solar-flare-like events from muon-like events.

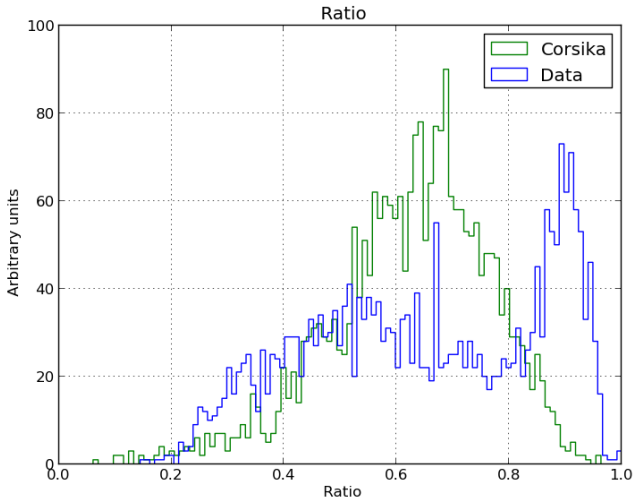

Figure 4.4: Comparison of the number of non-causally connected DOMs determined using *TWSRTOfflinePulses* over the total number of hit DOMs for data (blue) and Corsika (green). The behaviour of the two different sets of events is clearly different.

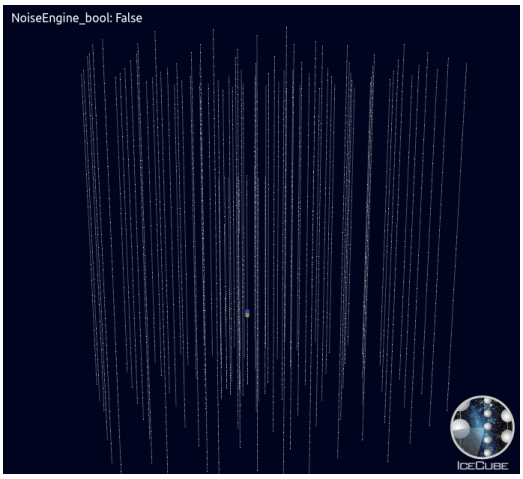

(a)

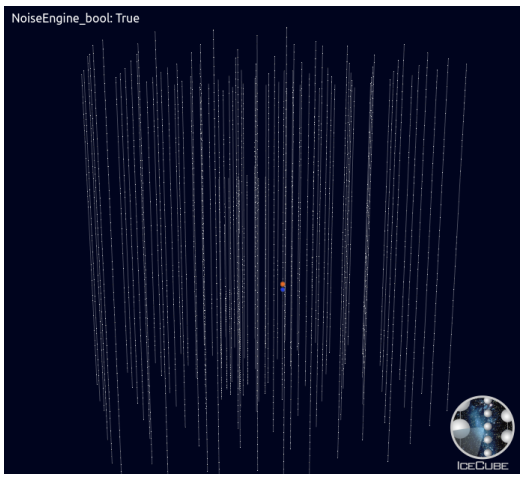

(b)

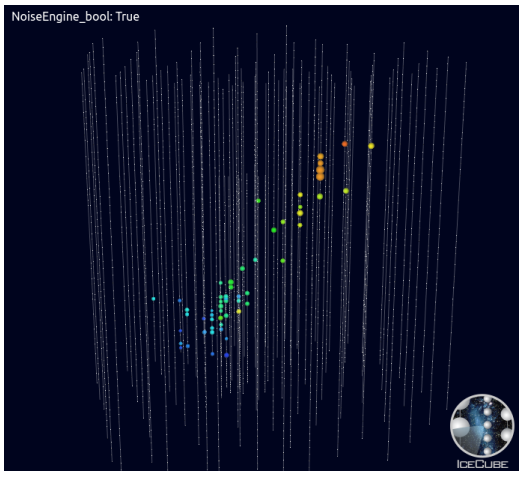

(c)

Figure 4.5: These Figures illustrate the causally connected DOMs determined by *TWSRTOfflinePulses* key for each kind of events in Figures 4.3. Figure 4.5(a) represents a noise event, the 4.5(b) one illustrates the solar-flare-like event while the 4.5(c) is a muon-like event.

One last cut !

After applying the "RATIO" cut, we have observed that some muon-like events still remained in the set of data. Figure 4.6 represents one of these events. It happens when the total number of hit DOMs is so large than even a large number of causally connected DOMs, due to a muon passing through the detector, does not push the RATIO below 0.75. An additional cut has therefore been added. It imposes fewer than x causally connected DOMs in each event i.e.

$$twsrt < x$$

x has to be small if we want that this cut gets rid of remaining muons. It is fixed in the following section.

The fine tuning of the threshold

The aim of this part of the analysis is to maximize the signal-noise-ratio (SNR). The signal comes from the MonteCarlo simulation files while the noise is given by data since they mostly contain atmospheric muons and noise events.
We applied cuts to the two sets of data using different cuts values. Table 4.1 shows the SNR obtained for the different cuts values. Detail about rates obtained for each file are presented in Appendix B.

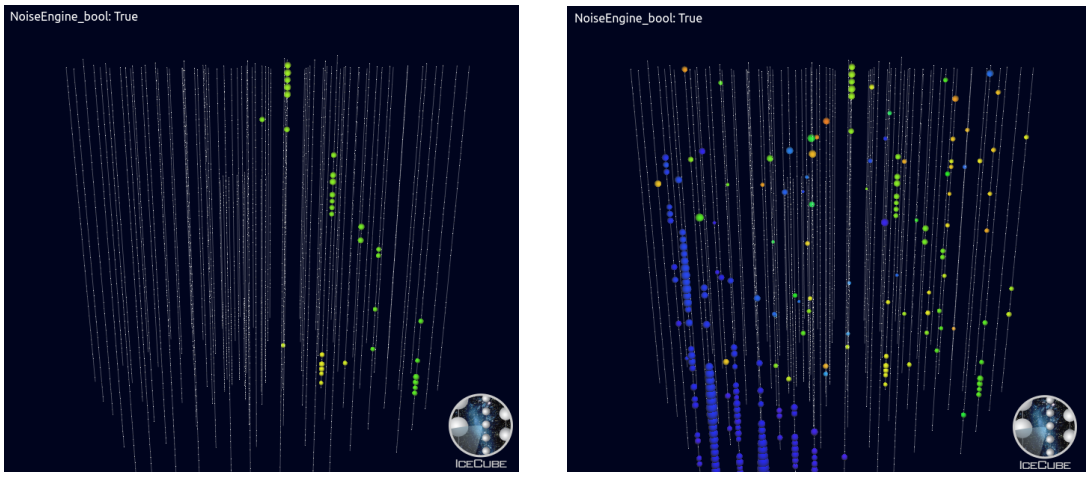

(a) (b)

Figure 4.6: These pictures represent the same event. The Figure 4.6(a) shows the causally connected DOMs. The Figure 4.6(b) contains all the hit DOMs. The total number of hit DOMs is significantly larger than the number of causally connected DOMs. The RATIO for this event is therefore close to 1.

	TWSRT	TWSRT	HiveSplitter
RATIO > 0.75			1.66
+ NoiseEngine cleaning	with	without	2.13
twsrt<8	1.64	1.42	
twsrt<6	1.52	1.26	
twsrt<5	1.29	1.09	
twsrt<4	0.33	0.89	
RATIO > 0.8			1.51
+ NoiseEngine cleaning	with	without	2.05
twsrt<8	1.58	1.54	
twsrt<6	1.48	1.26	
twsrt<5	1.29	1.09	
twsrt<4	0.91	0.77	

Table 4.1: This table presents the SNR for each possible cut value. The *HiveSplitter* column refers to the use of the *HiveSplitter* algorithm describes in Appendix A. The $twsrt < x$ mean that we impose there are less than x causally connected DOMs in each event. The blue value is the highest SNR i.e. the one which has been chosen.

4.2.1 The final choice

The chosen set of cuts values is

DeepCoreFilter passed	to make certain that events contain hit DOMs in the DeepCore.
RATIO > 0.75	to throw away most of muon-like events
NoiseEngine cleaning	to dump noise events
# twsrt < 8	to shed remaining muon-like events

The Figure 4.7 represents the deciding tree of filtering.

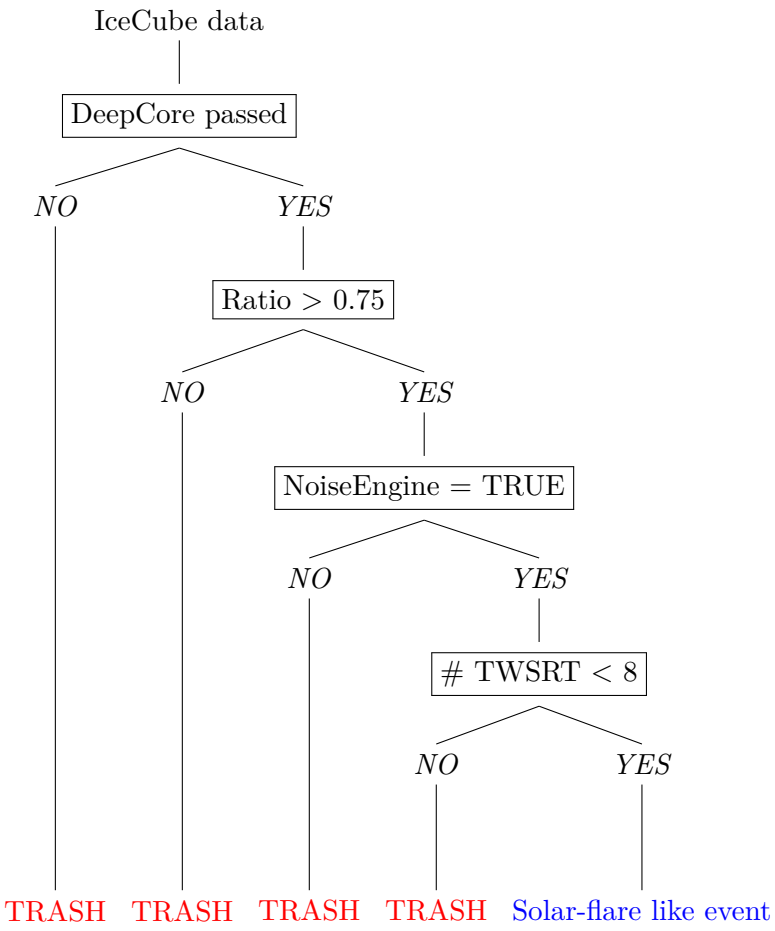

Figure 4.7: This deciding tree illustrates cuts used to extract solar-flare-like event from the entire set of IceCube data.

4.3 The chosen Solar Flares

As specified at the beginning of Section 4.2, we assume that solar flare neutrinos trigger the detector. It means that they have to be energetic enough. We have therefore worked with the most energetic flares i.e. the X flares (see Section 2.1.2). Table 4.2 shows the X flares which have been detected by GOES since the beginning of IC-86 (see Section 3.3) in March 2011 up to February 2012. We therefore analyse one year of data. Solar flares are presented according to their classifications and their date in Figure 4.8. The same analysis will also be carried out using M-flares.

Date	Start time	Peak time	End time	Classification
9 Aug 2011	07:48	08:05	08:08	X6.9
7 Sep 2011	22:32	22:38	22:44	X1.8
22 Sep 2011	10:29	11:01	11:44	X1.4
24 Sep 2011	09:21	09:40	09:48	X1.9
3 Nov 2011	20:16	20:27	20:32	X1.9
27 Jan 2012	17:37	18:37	18:56	X1.7

Table 4.2: List of solar flares classified as X from 03/2011 to 02/2012.

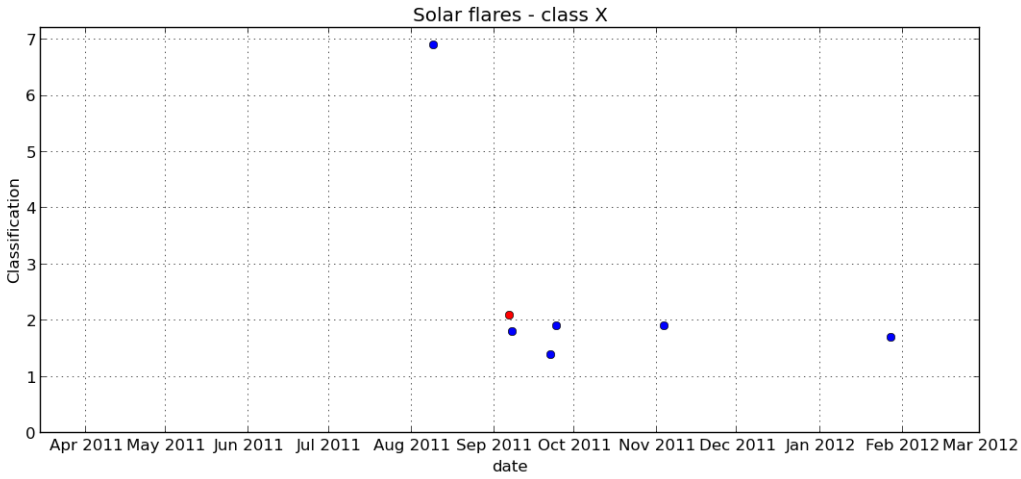

Figure 4.8: This plot shows the chosen solar flares according to their classification (X + number between 1.0 and 9.9) and their date. The red dot indicates that IceCube was not able to detect at this time.

4.4 Signal and background region definition

As detailed in Section 2.2.1, the X-rays start-times recorded by GOES represent, in this analysis, the start time of the flare. Given their close relationship with neutrinos due to their production channel, γ-rays end-times are used such as the end-times of the flares. Only the largest numbers of counts recorded by the Fermi satellite have been considered to evaluate the end-times.

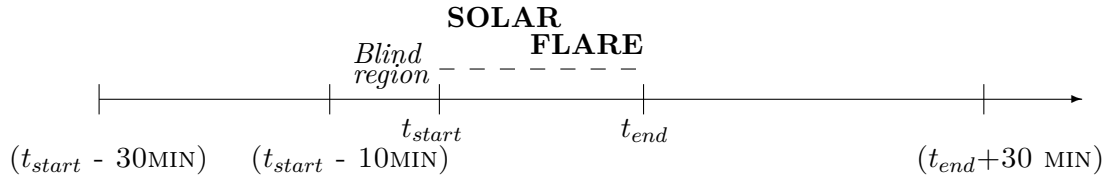

The t_{start} is so given by the GOES start time while the t_{end} is given by either Fermi data either GOES depending on which one is the later. IceCube data have been filtered from 30 minutes before the t_{end} until 30 minutes after the t_{end}. The blind region represents the last 10 minutes before the start time of the flare. We decided to blind this region in order to carry out an analysis the most model-independent as possible. We indeed do not know the arrival time of solar flare neutrinos and if, for some unknown reasons, they are detected before X-rays, they will be considered as background rather than solar flare signal. The blind region is not considered in the analysis. Considering 30 minutes before and after is an arbitrary choice that we made. These durations may be adapted.

Chapter 5

Results

5.1 Solar Flares analysis

Six flares are analysed in this chapter. They correspond to one year of data: from March 2011 to February 2012. The analysis is described for the first flare in Section 5.1.1. The analyses of the other flares are made in the same way. All results are also presented together in Appendix C.

5.1.1 X6.9 Solar Flare - 09/08/2011

Characteristics of the flare

- Classification : X6.9
- Region : 11263 (see Figure 5.1)
  The region where the flare occured may be important. We expect indeed a different neutrino flux from flare occuring in the center of the side of the Sun or from a limb flare as explained in Section 4.1.
- GOES data (UTC):
  - Start-time : 07:48
  - End-time : 08:08
  - duration : 20 minutes
- Fermi data (UTC):
  - Start-time : 07:49
  - End-time : 08:24
  - duration : 35 minutes

  As described in Section 4.4, X-rays and γ-rays detections play an important role in this analysis: they set the time considered. For this flare, data are filtered

from (07:48 - 30 min = 07:18) until (08:24 + 30 min = 08:54). The end time is determined by either the X-rays end time either the γ-rays end time depending on which is the later.

- previous flare : C1.4 ending at 07:27
- next flare : C2.2 starting at 13:29

  We have no idea of the start time of neutrino production and therefore neither of the arrival time of these neutrinos. It is therefore important to know what is the neighbourhood of the considered flare in order to know where our signal might come from. This information is not important at this step of the analysis because we do not know if we will detect neutrinos coming from M or C flares.

Neutrino oscillations

Earth-Sun distance : 1.0139 UA

The Earth-Sun distance varies depending on the time of year. It is important to know this distance as precisely as possible to evaluate the oscillation probabilities.

ν_μ	$P(\nu_\mu \to \nu_\mu)$	=	0.3336
	$P(\nu_\mu \to \nu_\tau)$	=	0.3593
	$P(\nu_\mu \to \nu_e)$	=	0.3070
ν_e	$P(\nu_e \to \nu_\mu)$	=	0.3070
	$P(\nu_e \to \nu_\tau)$	=	0.1685
	$P(\nu_e \to \nu_e)$	=	0.5244

This table represents the oscillation probabilities for a ν_μ and for a ν_e which are produced in the chromosphere. There is a large fraction of ν_τ expected. See the implication on the detection rate in Section 4.1.

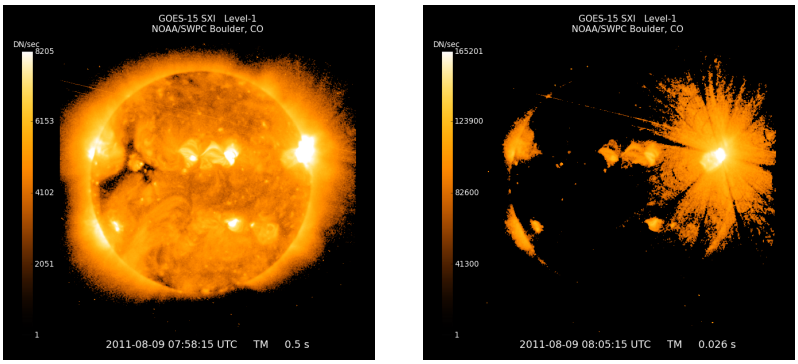

(a) (b)

Figure 5.1: X6.9 Solar Flare - 09/08/2011. It occurred in region 11263 (first quadrant on this Figure considering an anti-clockwise). Image credit : GOES

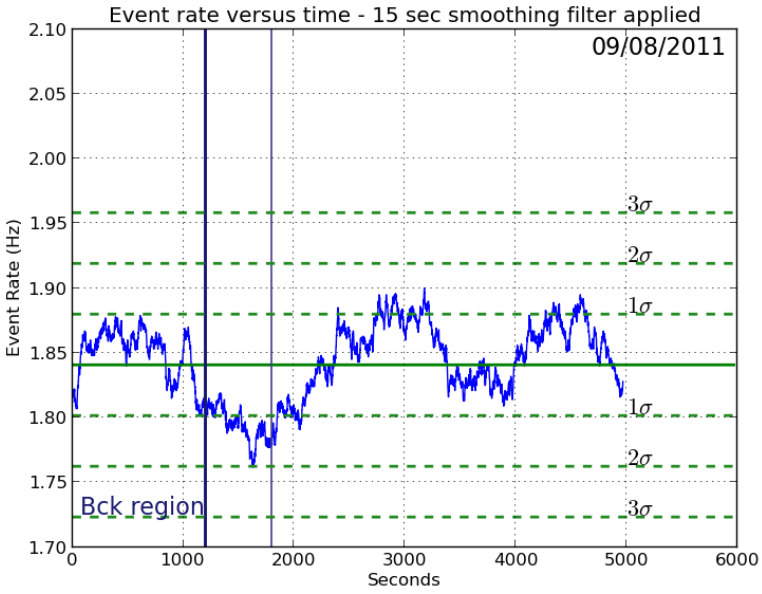

Figure 5.2: This plot shows the event rate versus the time. "Bck region" represents the first 20 minutes which are used to evaluate the background. This region ends at the vertical blue line. The thinner and lighter blue line shows the start time of the flare. The region between the two blue lines is what we called the blind region in Section 4.4. The green line represents the mean value of the background region and the green dashed lines represent 1, 2 and 3 standard deviations.

5.1.2 X1.8 Solar Flare - 07/09/2011

Characteristics of the flare

- Classification : X1.8
- Region : 11283 (see Figure 5.3)
- GOES data (UTC):
  - Start-time : 22:32
  - End-time : 22:44
  - duration : 12 minutes
- Fermi data (UTC):
  - Start-time : 22:34
  - End-time : 22:41
  - duration : 7 minutes
- previous flare : C1.6 ending at 22:26
- next flare : C1.7 starting at 10:40 (08/09/2011)

Neutrino oscillations

Earth-Sun distance : 1.0077 UA

ν_μ	$P(\nu_\mu \to \nu_\mu)$	=	0.3190
	$P(\nu_\mu \to \nu_\tau)$	=	0.3662
	$P(\nu_\mu \to \nu_e)$	=	0.3148
ν_e	$P(\nu_e \to \nu_\mu)$	=	0.31488
	$P(\nu_e \to \nu_\tau)$	=	0.1743
	$P(\nu_e \to \nu_e)$	=	0.5108

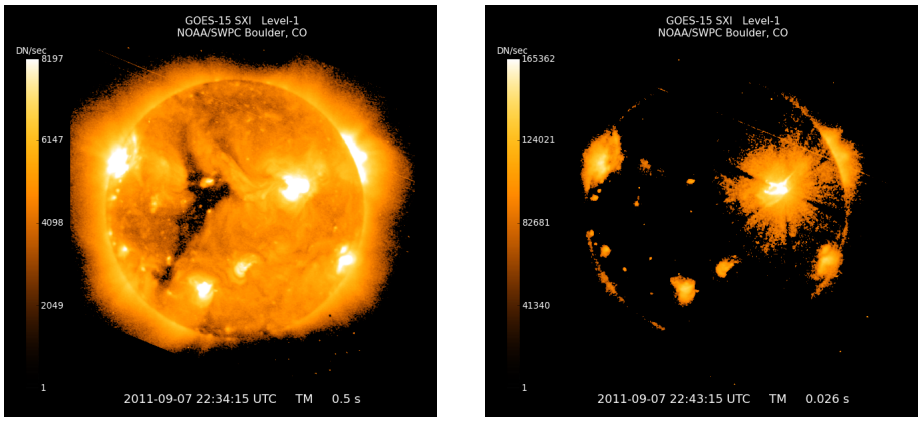

(a) (b)

Figure 5.3: X1.8 Solar Flare - 07/09/2011. It occurred in region 11283 (first quadrant on this Figure). Image credit : GOES

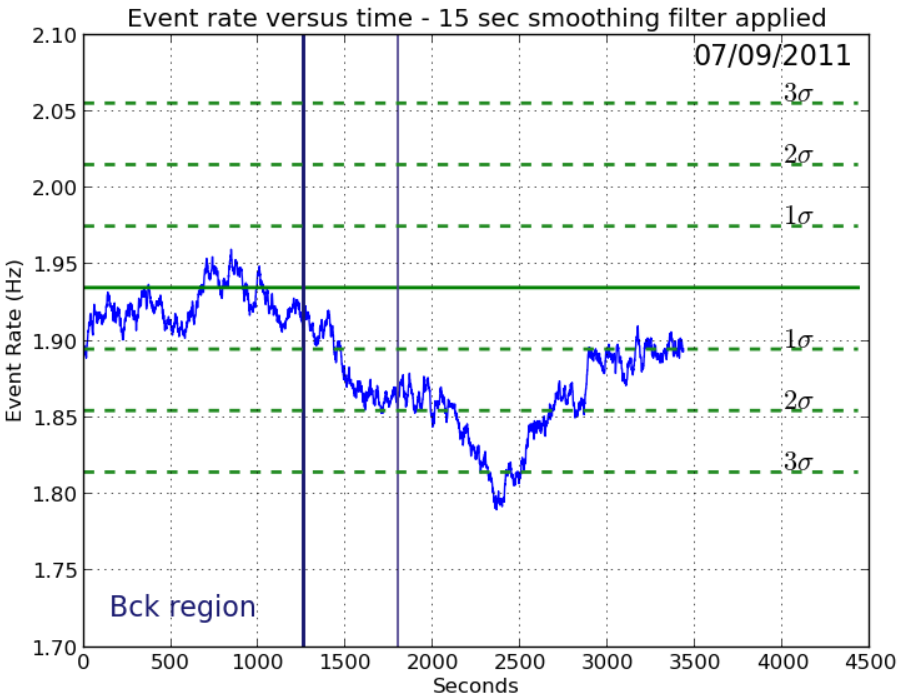

Figure 5.4: Event rate versus time - 07/09/2011

5.1.3 X1.4 Solar Flare - 22/09/2011

Characteristics of the flare

- Classification : X1.4
- Region : 11302 (see Figure 5.3)
- GOES data (UTC):
  - Start-time : 10:29
  - End-time : 11:44
  - duration : 75 minutes
- Fermi data (UTC):
  - Start-time : 11:09
  - End-time : 11:46
  - duration : 37 minutes
- previous flare : M1.1 ending at 10:09
- next flare : C4.0 starting at 20:14

Neutrino oscillations

Earth-Sun distance : 1.0038 UA

ν_μ	$P(\nu_\mu \to \nu_\mu)$	=	0.3025
	$P(\nu_\mu \to \nu_\tau)$	=	0.3963
	$P(\nu_\mu \to \nu_e)$	=	0.3011
ν_e	$P(\nu_e \to \nu_\mu)$	=	0.3011
	$P(\nu_e \to \nu_\tau)$	=	0.1732
	$P(\nu_e \to \nu_e)$	=	0.5256

Remarks

Figure 5.6 does not show the background region which correspond to a change of run in IceCube data. During a change of run, IceCube is blind during about 60 s. We therefore retrieved 75 s from the background time and we did not count events during this time. The mean value represented in green has been evaluated without these 75 s.

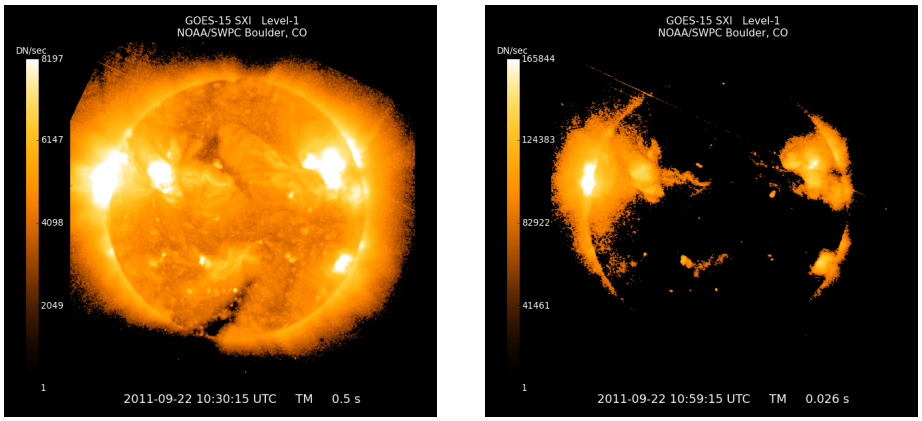

(a) (b)

Figure 5.5: X1.4 Solar Flare - 22/09/2011. It occurred in region 11302 (second quadrant on this Figure). Image credit : GOES

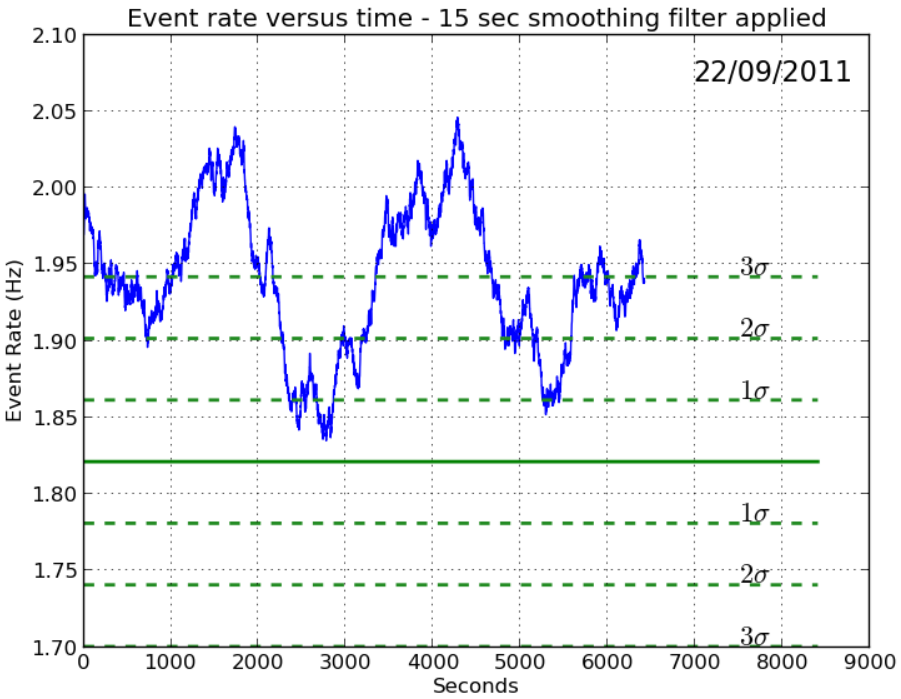

Figure 5.6: Event rate versus time - 22/09/2011

5.1.4 X1.9 Solar Flare - 24/09/2011

Characteristics of the flare

- Classification : X1.9
- Region : 11302 (see Figure 5.7)
- GOES data (UTC):
  - Start-time : 09:21
  - End-time : 09:48
  - duration : 27 minutes
- Fermi data (UTC):
  - Start-time : 09:31
  - End-time : 09:51
  - duration : 20 minutes
- previous flare : C2.2 ending at 108:55
- next flare : C2.7 starting at 11:25

Neutrino oscillations

Earth-Sun distance : 1.0032 UA

ν_μ	$P(\nu_\mu \to \nu_\mu)$	=	0.3606
	$P(\nu_\mu \to \nu_\tau)$	=	0.3812
	$P(\nu_\mu \to \nu_e)$	=	0.2581
ν_e	$P(\nu_e \to \nu_\mu)$	=	0.2581
	$P(\nu_e \to \nu_\tau)$	=	0.1605
	$P(\nu_e \to \nu_e)$	=	0.5813

Remarks

Figure 5.8 does not show results for the period after the end time of the flare because of a change of run.

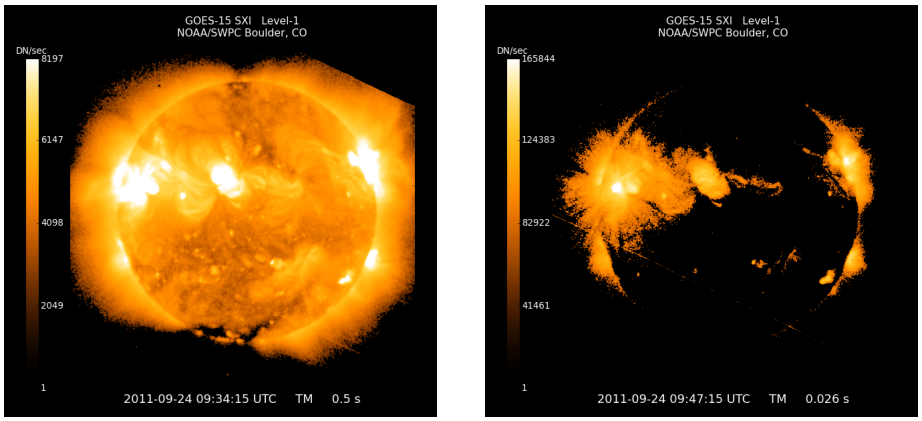

(a) (b)

Figure 5.7: X1.9 Solar Flare - 24/09/2011. It occurred in region 11302 (second quadrant on this Figure). Image credit : GOES

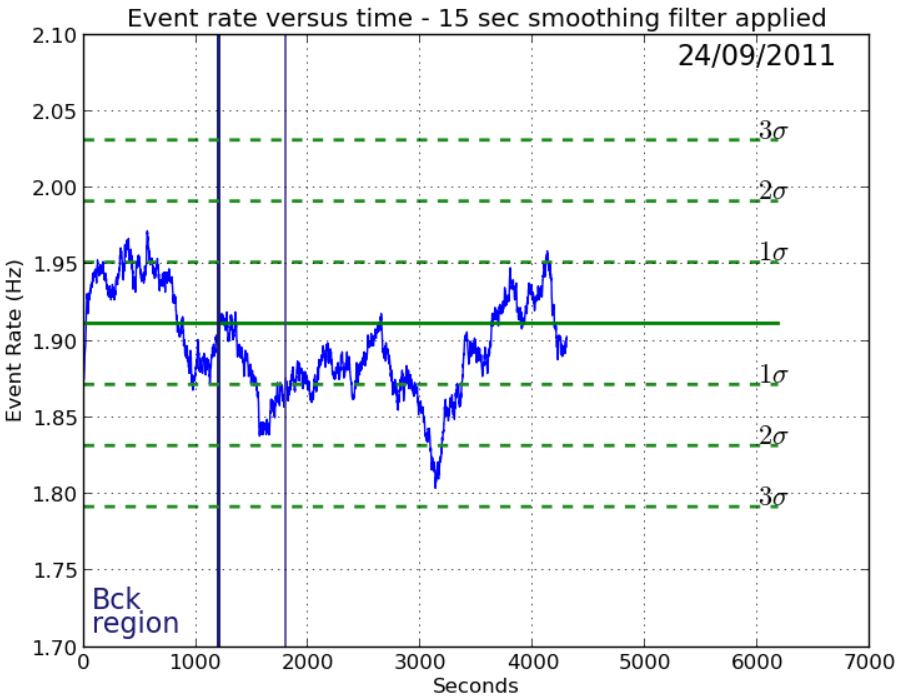

Figure 5.8: Event rate versus time - 24/09/2011

5.1.5 X1.9 Solar Flare - 03/11/2011

Characteristics of the flare

- Classification : X1.9
- Region : 11339 (see Figure 5.9)
- GOES data (UTC):
  - Start-time : 20:16
  - End-time : 20:32
  - duration : 16 minutes
- Fermi data (UTC):
  - no strong detection by Fermi
- previous flare : C4.5 ending at 19:00
- next flare : C5.4 starting at 22:12

Neutrino oscillations

Earth-Sun distance : 0.9920 UA

ν_μ	$P(\nu_\mu \to \nu_\mu)$	=	0.3754
	$P(\nu_\mu \to \nu_\tau)$	=	0.3758
	$P(\nu_\mu \to \nu_e)$	=	0.2488
ν_e	$P(\nu_e \to \nu_\mu)$	=	0.2488
	$P(\nu_e \to \nu_\tau)$	=	0.1456
	$P(\nu_e \to \nu_e)$	=	0.6055

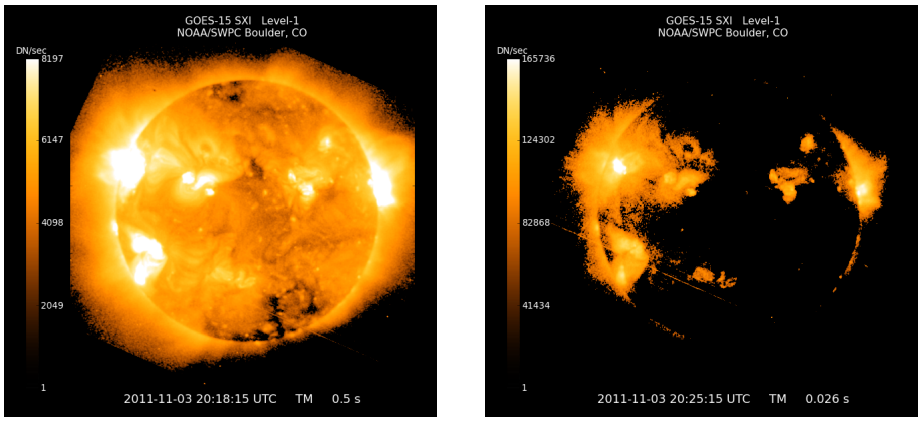

(a) (b)

Figure 5.9: X1.9 Solar Flare - 03/11/2011. It occurred in region 11339 (second quadrant on this Figure). Image credit : GOES

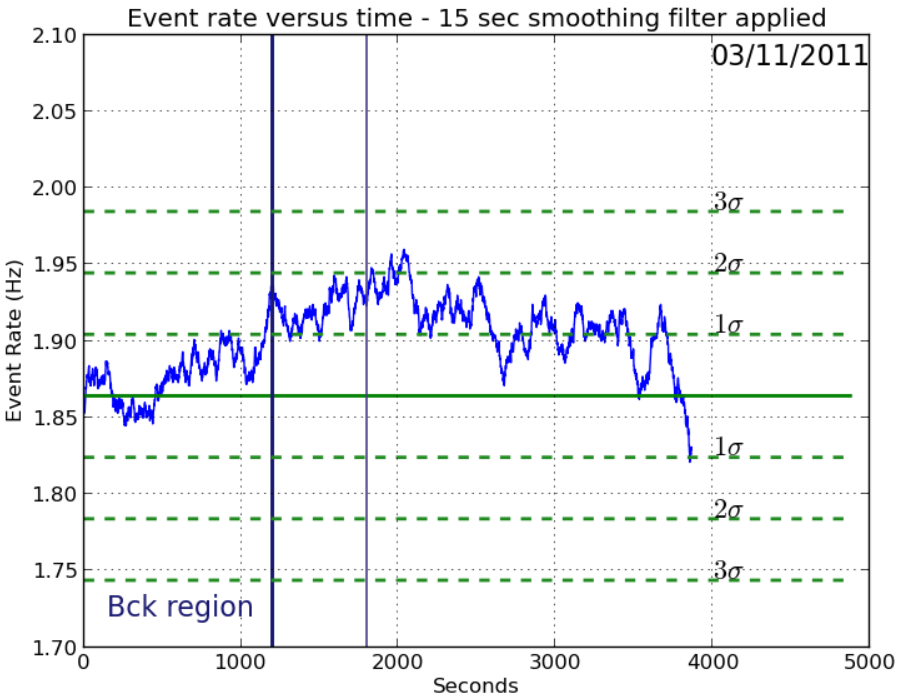

Figure 5.10: Event rate versus time - 03/11/2011

5.1.6 X1.7 Solar Flare - 27/01/2012

Characteristics of the flare

- Classification : X1.7
- Region : 11402 (see Figure 5.11)
- GOES data (UTC):
  - Start-time : 17:37
  - End-time : 18:56
  - duration : 79 minutes
- Fermi data (UTC):
  - Start-time : 17:45
  - End-time : 18:15
  - duration : 30 minutes

  - Start-time : 18:34
  - End-time : 18:44
  - duration : 10 minutes
- previous flare : C1.0 ending at 13:09
- next flare : C1.0 starting at 15:30 (28/01/2012)

Neutrino oscillations

Earth-Sun distance : 0.9847 UA

ν_μ	$P(\nu_\mu \to \nu_\mu)$	=	0.3385
	$P(\nu_\mu \to \nu_\tau)$	=	0.3743
	$P(\nu_\mu \to \nu_e)$	=	0.2872
ν_e	$P(\nu_e \to \nu_\mu)$	=	0.2872
	$P(\nu_e \to \nu_\tau)$	=	0.1755
	$P(\nu_e \to \nu_e)$	=	0.5373

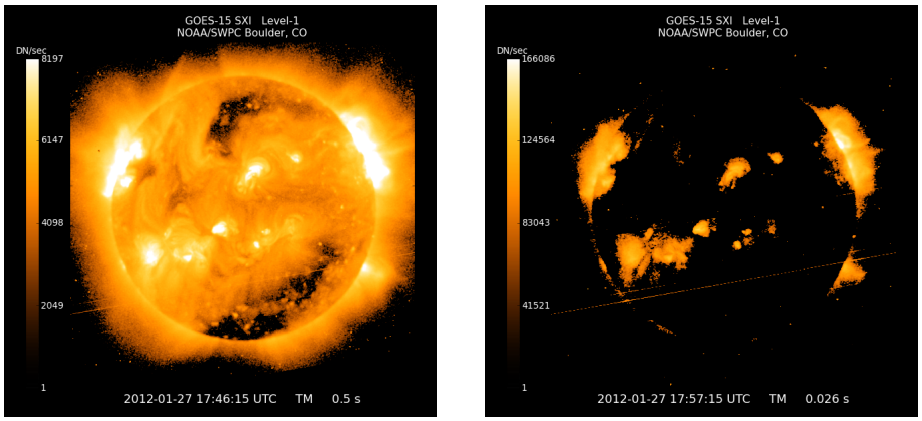

(a) (b)

Figure 5.11: X1.7 Solar Flare - 27/01/2012. It occurred in region 11402 (first quadrant on this Figure) Image credit : GOES

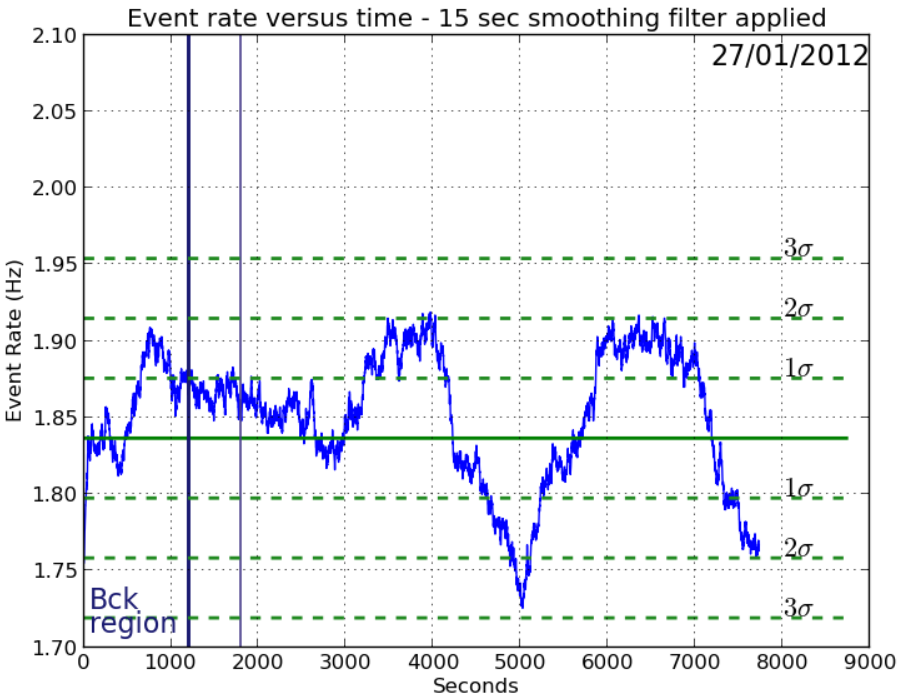

Figure 5.12: Event rate versus time - 27/01/2012

5.2 Stacking analysis

In this section we will sum all results which have been obtained for each solar flare presented in the previous section. Results presented in the following table are obtained in the following way :

- The *Background region* is the sum of the number events N_{bck} during the background time t_{bck} for each flare divided by the background time t_{bck} multiplied by the time of the flare t_{fl}

$$\text{Background region} = \sum_{\text{flares}} \frac{N_{bck}}{t_{bck}} t_{fl}$$

- The *Flare region* is the sum of the number events N_{fl} during the flare time t_{fl} for each flare

$$\text{Flare region} = \sum_{\text{flares}} N_{fl}$$

- The *"Flare and after" region* is the sum of the number events N_{fl} during the flare time t_{fl} and the number of events N_{aft} during the 30 minutes considered after the end time (see section 4.4) for each flare

$$\text{"Flare and after" region} = \sum_{\text{flares}} N_{fl} + N_{aft}$$

  The associated *Background region* is obtained following

$$\text{Background region} = \sum_{\text{flares}} \frac{N_{bck}}{t_{bck}} (t_{fl} + t_{aft})$$

  where t_{aft} is the time of the after region (i.e. 30 minutes).

N_{bck}, N_{fl}, N_{aft} and their corresponding time for each flare are presented in the following table.

Background region	Flare region
28110	28255
Background region	**"Flare and after" region**
48465	48364

Flare	t_{bck}(s)	N_{bck}	t_{fl}(s)	N_{fl}	R_{fl}(Hz)	t_{aft}(s)	N_{aft}
09/08/2011	1200	2222	2160	3958	1.83	1800	3305
07/09/2011	1200	2325	720	1341	1.86	1800	3357
22/09/2011	1125	2087	4620	8961	1.94	1800	3447
24/09/2011	1200	2298	1800	3380	1.88	1800	3285
03/11/2011	1200	2244	960	1860	1.94	1800	3404
27/01/2012	1200	2203	4740	8755	1.85	1800	3311

Table 5.1: N_{bck}, N_{fl}, N_{aft} and their corresponding time for each flare

The Background time is shorter for the solar flare which occurred on the 22/09/2011 because of a change in IceCube run as already pointed out in Section 5.1.

5.3 Discussion

From the individual flare analysis presented in Section 5.1, we observe no commonality between results behaviour. If a dominant behaviour has to be found, we would say that we observe an anti-correlation between solar flare events and data recorded by IceCube. Moreover being in total opposition that models' predictions, we do not see a physical reason which explained this anti-correlation. Further investigation are therefore required.

There is no significant effect that can be extract from the stacking analysis since there is an excess in the flare region smaller than one standard deviation.

$$\text{Flare region} - \text{Background region} = 28255 - 28110 = 145$$

while

$$1\sigma = \sqrt{\text{Background region}} = \sqrt{28110} = 168$$

The reader has noted that the 22/09/2011 flare presents an increase in the flare region compared to the background region. More investigation are required before making any conclusion: more data will be filtered before but mainly after the flare region.

It is interesting to note that the number of events in the background region - presented in Table 5.1 - is nearly constant for each flare with about 2253 events during 1200 s. It means that the filtering process gets rid of most of the atmospheric muons. A seasonal difference should indeed be observed if the background was dominated by atmospheric muons [12].

Conclusion and Outlook

The aim of the master thesis presented here consisted of a search for GeV neutrinos coming from solar flares in IceCube - or more precisely in DeepCore. The first step of this search was to determine the sensitivity of the DeepCore to solar flare neutrinos. The main issue in this task was to determine the neutrino flux expected from solar flares. Several models are indeed proposed in theory and their results are completely divergent. We decided to choose the most optimistic model. According this model and after an evaluation of the IceCube DeepCore background, the number of expected cascades produced by a single large flare is larger than that required for a 3σ detection.

Then, a filtering process has been developed. The filtering process had to be able to get rid of atmospheric muons - which constitute the most numerous events recorded by IceCube - but also get rid of what we called noise events. Different parameters have been tested and the final cut has been shown in Section 4.2.1.

Using this filtering process, an analysis of one year of IceCube data (from March 2011 until February 2012) has been conducted. We decided to compare IceCube data with X-solar flares since we made the assumption that solar flare neutrinos will trigger the detector. Given the lack of a solar flare model for neutrino production, a model-independent data analysis has been chosen: the start time of the flare was determined using the start time of the X-rays detection by the Geostationary Operational Environmental Satellite (GOES) while the end time of the flare came from either the end time of GOES detection either the one of the γ-rays detection by the Fermi satellite depending on the later detection. IceCube data have been filtered from 30 minutes before this start time until 30 minutes after this end time. We respectively called each region the "Background region", the "Flare region"and the "After region". The last 10 minutes of the Background region have been blinded in order to prevent pollution of this region by a possible early solar flare neutrino flux. Two different ways to analyse the data were presented: an individual solar flare analysis and a stacking analysis. The former consisted of search for an increase in the filtered data rate in the flare region while the latter sum up results obtained in each region for each individual flare.

As explained in Chapter 5, the final set of data has been cleaned of most of the atmospheric muons since no season variation are observed in the Background region.

We cannot extract a general behaviour of the Flare region from the individual solar flare analysis even if a slight anti-correlation between solar flares and filtered data might be observed. In addition to disagree with current models of neutrino production in solar flares, we cannot find a physical phenomenon which could explain this result. Further investigations are therefore required before concluding. The flare which occurred on the 22^{nd} September 2011 presents a peculiar behaviour with a clear increase in the filtered data rate in the Flare region. We plan to filter more data after the end of the After region to see what happens next before concluding.

The next step will consist of the filtering and analysis of IceCube data from March 2012 until now. We are currently in the maximum of the 24^{th} of the 11-year-solar cycle. Data of this period are therefore of great interest. A search for neutrinos coming from solar flares with a different classification has also to be conducted. In this way an upper-limit on the neutrino flux produced by different classes of solar flares will be obtained.

This master thesis constitutes a first step in the search for solar flare neutrinos using IceCube or its extensions. One of these planned extensions - the Precision IceCube Next Generation Upgrade (PINGU) - is dedicated to the energy region between a few GeV to 50 GeV. Although it was originally dedicated to neutrino oscillation studies, the PINGU design is generally a very large volume neutrino detector with the ability to veto cosmic ray background using the surrounding IceCube detector and an ability to reconstruct energy down to GeV-scale. As such it would improve any measurements of solar neutrinos using the improvement in energy resolution and the reduction of systematic uncertainties. Indeed, the denser instrumentation of PINGU compared to DeepCore, is expected to enhance the full array's sensitivity to very low energy.

An analysis of the correlation between IceCube/PINGU data and solar flares coming from the hidden side of the Sun will be also carried out. Since this side is invisible for optical observations, an exact coincidence with neutrino data can not be defined. Nevertheless, a correlation between the number of solar flares and neutrino events integrated over a large time period will provide additional information in the solar flare description. The study of solar flares on the side of the Sun opposite to Earth can also improve our understanding of neutrino oscillations. These neutrinos have indeed to cross the solar core before they reach the Earth and so the MSW mechanism will play an important role.

As explained in Section 2.3.2, neutrinos coming from solar flares constitute an unique insight in the hadron acceleration in solar flares and may therefore lead to an experimental characterization of the acceleration mechanisms. For example, a timing comparison between the data of X-ray emissions from solar flares, recorded by satellites such as GOES, and data obtained by IceCube would provide the delay between electron and hadron acceleration in the case of detection. Depending on the acceleration mechanism considered, the hadron acceleration can differ from the electron acceleration. Hence information about a possible delay should already let us to reject some of the acceleration

mechanisms proposed by theory.

To conclude, we can say that, even if we are not able to fix an upper limit on the neutrino flux coming from solar flares to date, this master thesis constitute a step forward the possible detection of these neutrinos by IceCube, the South Pole Neutrino Observatory.

Appendices

Appendix A

Graphs related to the non-chosen parameters

Parameter linked to distance between reconstructed track and hit DOMs.

The first tested parameter was in relation with the reconstructed track. The shortest distance between this track and each hit DOM in the event was evaluated and the ratio between this number and the total number of hit DOMs was then computed. This work has been done for two different fits : LineFit and MPEFit. Results are presented in Figures A.1(a) and A.1(b). This parameter does not provide interesting result since there is no clear difference in the behaviour of data and Corsika.

Parameter linked to the DOMs' causality

The number of non-causally connected DOMs has been studied for data and Corsika. This number is obtained computing the difference between the *OfflinePulses* and the *TWSRTOfflinePulses* (see Section 4.2). The behaviour of the different sets of events can be seen in Figure A.2. There is no clear difference between data and Corsika that can be found. Therefore this parameter has not been chosen.

Parameter linked with the DOMs' causality - *HiveSplitter*

HiveSplitter is an algorithm which determines in each event a set of causally connected DOMs. This algorithm is, in general, less restrictive than the *TWSRTOfflinePulses* one. The parameter studied here is a ratio similar to the one developed in Section 4.2 i.e. the number of non-causally connected DOMs defined using *HiveSplitter* over the total number of hit DOMs. Although there is a clear difference between data and Corsika behaviour regard to this parameter, we decided to do not use it. *HiveSplitter* is a rather new algorithm, it is so less tested than the old *TWSRTOfflinePulses* one. A study of its

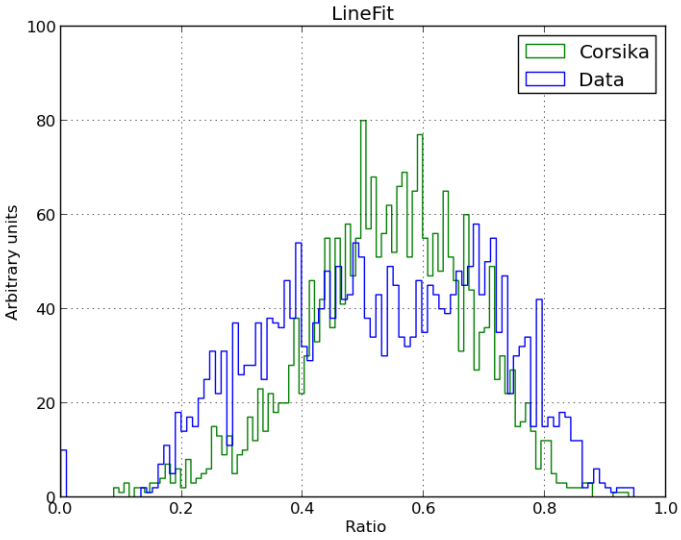

(a)

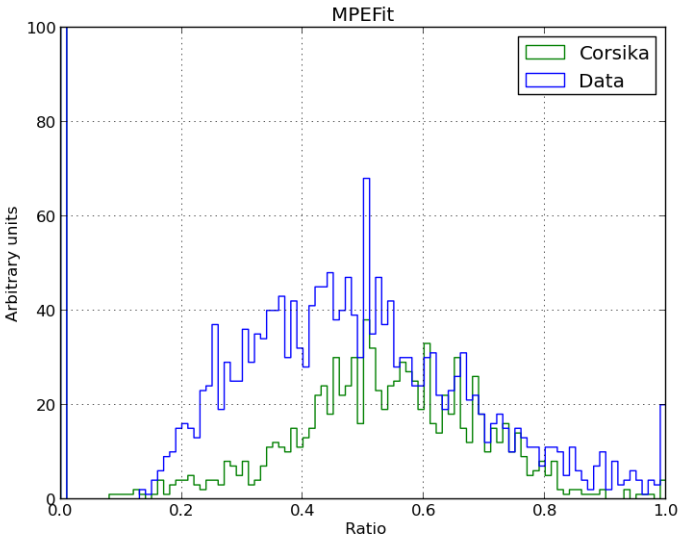

(b)

Figure A.1: Behaviour of data (blue) and Corsika (green) in function of the ratio parameter linked with the distance between reconstructed track and hit DOMs. The LineFit recontruction is considered in Figure A.1(a) while Figure A.1(b) is the result for MPEFit.

reaction with MonteCarlo simulation files will be carried on in the future. The behaviour of the sets of events is presented in Figure A.3.

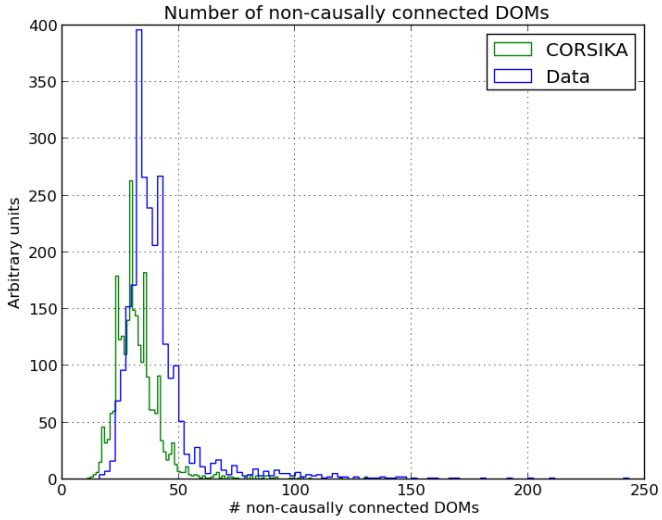

Figure A.2: Comparison of the number of non-causally connected DOMs for data (blue) and Corsika (green)

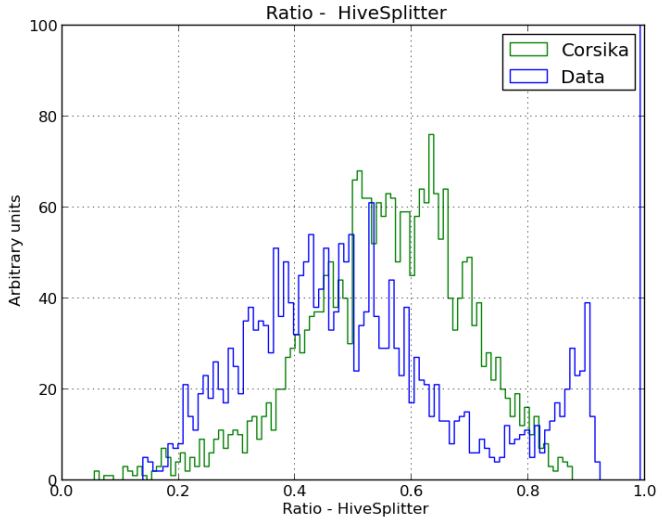

Figure A.3: Comparison of the number of non-causally connected DOMs determined using *HiveSplitter* over the total number of hit DOMs for data (blue) and Corsika (green)

Appendix B

Rate for each set of events according to the cuts values

B.1 DATA

		TWSRT	TWSRT	HiveSplitter
Initial file	26 Hz			
RATIO > 0.75		10Hz		7.36Hz
	+ NoiseEngine cleaning	with	without	1.35Hz
	twsrt<8	1.73Hz	7.59Hz	
	twsrt<6	1.12Hz	6.40Hz	
	twsrt<5	0.77Hz	5.16Hz	
	twsrt<4	0.42Hz	3.26Hz	
RATIO > 0.8		8.77Hz		6.81 Hz
	+ NoiseEngine cleaning	with	without	1.16Hz
	twsrt<8	1.68Hz	7.49Hz	
	twsrt<6	1.12Hz	6.40Hz	
	twsrt<5	0.77Hz	5.16Hz	
	twsrt<4	0.42Hz	3.26Hz	

B.2 Corsika

		TWSRT	HiveSplitter
Initial file	485Hz		
RATIO > 0.75		82Hz	26Hz
	twsrt<8	36Hz	
	twsrt<6	11Hz	
	twsrt<5	1.59Hz	
	twsrt<4	0Hz	
RATIO > 0.8		38Hz	9Hz
	twsrt<8	25Hz	
	twsrt<6	9.68Hz	
	twsrt<5	1.59Hz	
	twsrt<4	0Hz	

B.3 CLsim

		TWSRT	TWSRT	HiveSplitter
file114/115	99/99 events			
RATIO > 0.75		91/93	91/93	87/89
	+ NoiseEngine cleaning	with	without	52/48
	twsrt<8	51/41	87/82	
	twsrt<6	33/31	63/62	
	twsrt<5	22/22	49/50	
	twsrt<4	10/11	32/34	
RATIO > 0.8		76/79	76/79	76/73
	+ NoiseEngine cleaning	with	without	41/35
	twsrt<8	41/37	76/77	
	twsrt<6	32/31	62/62	
	twsrt<5	22/22	49/50	
	twsrt<4	10/11	32/34	

Appendix C

Solar Flare analysis : details

Here follows the results of the individual analysis carried out for each flare. These plots show the event rate versus the time. "Bck region" represents the first 20 minutes which are used to evaluate the background. This region ends at the vertical blue line. The thinner and lighter blue line shows the start time of the flare. The region between the two blue lines is what we called the blind region in section 4.4. The green line represents the mean value of the background region and the green dashed lines represent 1, 2 and 3 standard deviations.
Figure C.1(c) does not show the background region which correspond to a change of run in IceCube data. During a change of run, IceCube is blind during about 60 s. We therefore retrieved 75 s from the background time and we did not count events during this time. The mean value represented in green has been evaluated without these 75 s.
Figure C.1(d) does not show results for the period after the end time of the flare because of a change of run.

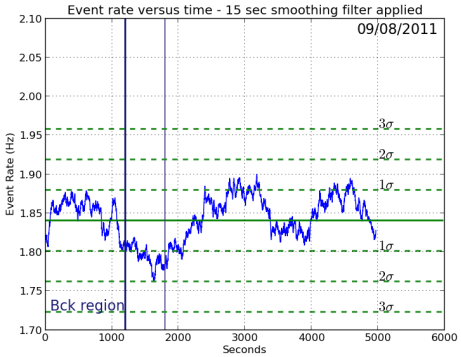
Event rate versus time - 15 sec smoothing filter applied
09/08/2011
Event Rate (Hz)
Seconds
Bck region
3σ
2σ
1σ

(a)

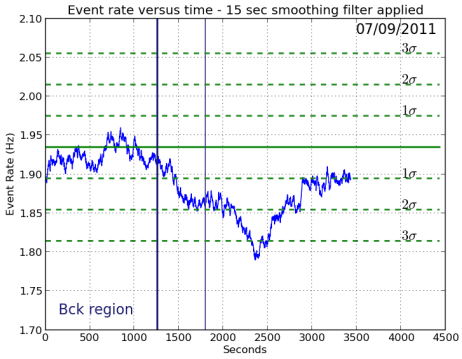
Event rate versus time - 15 sec smoothing filter applied
07/09/2011
Event Rate (Hz)
Seconds
Bck region
3σ
2σ
1σ

(b)

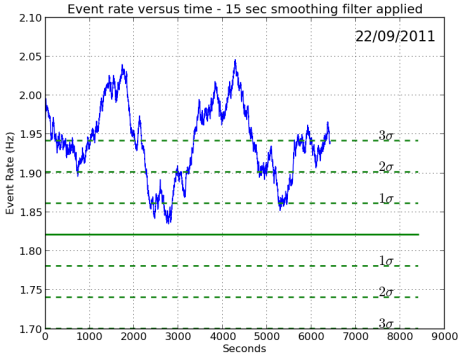
Event rate versus time - 15 sec smoothing filter applied
22/09/2011
Event Rate (Hz)
Seconds
3σ
2σ
1σ

(c)

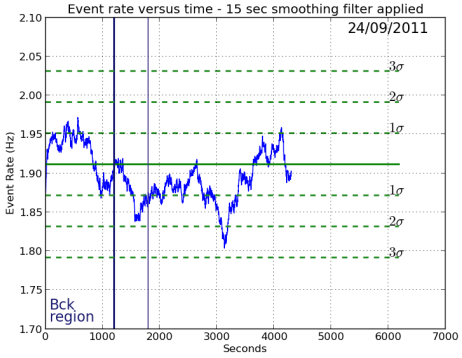
Event rate versus time - 15 sec smoothing filter applied
24/09/2011
Event Rate (Hz)
Seconds
Bck
region
3σ
2σ
1σ

(d)

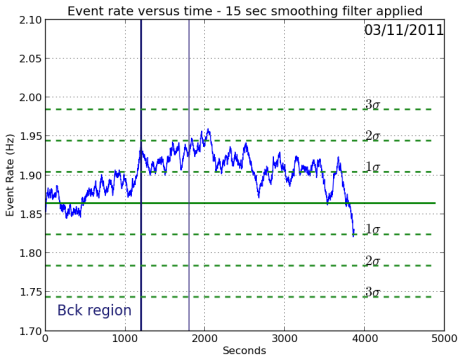
Event rate versus time - 15 sec smoothing filter applied
03/11/2011
Event Rate (Hz)
Seconds
Bck region
3σ
2σ
1σ

(e)

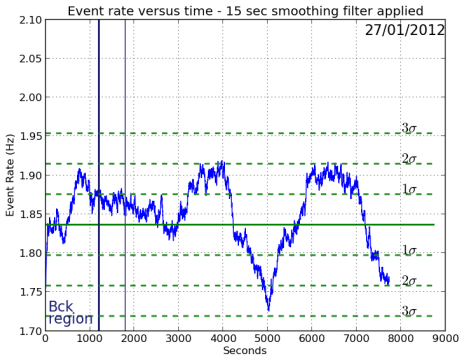
Event rate versus time - 15 sec smoothing filter applied
27/01/2012
Event Rate (Hz)
Seconds
Bck
region
3σ
2σ
1σ

(f)

Bibliography

[1] The Transition Region and Coronal Explorer. *http://trace.lmsal.com/*.

[2] National Aeronautics and Space Administration. Solar Physics - Marshall Space Flight Center. *http://solarscience.msfc.nasa.gov/predict.shtml*.

[3] RESOLUTION B2. RESOLUTION B2 on the re-definition of the astronomical unit of length. Beijing, Kina: International Astronomical Union, 31 August 2012, retrieved 2012-09-19.

[4] John N. Bahcall. Solar Flares and Neutrino Detectors. *Physical Review Letters*, 61(23):2650:2652, 1988.

[5] A. O. Benz and M. Güdel. Physical Processes in Magnetically Driven Flares on the Sun, Stars, and Young Stellar Objects. *Annual Review of Astronomy and Astrophysics*, 48:241–287, 2010.

[6] J. Bouchez. Neutrinos. In D. Kazakov and G. Smadja, editors, *Particle Physics and Cosmology: The Interface*, volume II. Mathematics, Physics and Chemistry - Vol. 188 of *NATO Sciences Series*, pages 111–170, 2008.

[7] Steve Boyd. Neutrino Oscillations. 2013.

[8] J.J.Gómez Cadenas and F.Monrabal. Francis Halzen: "I always advise to my students 'don't read too many books, do things!'". 2014. *http://www.jotdown.es/2014/05/francis-halzen-i-always-advise-to-my-students-dont-read-too-many-books-do-things/*.

[9] The Center for Science Education at the UC Berkeley Space Sciences Laboratory. Coronal Weather Report. Part of the LIVING WITH A STAR project. *http://cse.ssl.berkeley.edu/coronalweather/intro.html*.

[10] J. Chadwick. Possible Existence of a Neutron. *Nature*, page 129:312, 1932.

[11] E. L. Chupp and J. M. Ryan. High Energy Neutron and Pion-decay Gamma-ray Emissions from Solar Flares. *Research in Astronomy and Astrophysics*, 9(1):11–40, November 2008.

[12] IceCube Collaboration. Atmospheric Variations as observed by Icecube. PROCEEDINGS OF THE 31st LODZ ICRC, 2009 *arXiv:1001.0776 [astro-ph.HE]*.

[13] IceCube collaboration. Hard Local Coincidence. *Available on IceCube wikipage*.

[14] IceCube collaboration. Optical properties of deep glacial ice at the South Pole. *Journal of Geophysical Research: Atmospheres*, 111, 2006. Issue D13.

[15] IceCube Collaboration. The Design and Performance of IceCube DeepCore. 2011. *arXiv:1109.6096 [astro-ph.IM]*.

[16] IceCube Collaboration. Evidence for High-Energy Extraterrestrial Neutrinos at the Icecube Detector. *Science*, 342, 2013.

[17] LAT Collaboration. The Large Area Telescope on the Fermi Gamma-ray Space Telescope Mission. *arXiv:0902.1089 [astro-ph.IM]*.

[18] SNO Collaboration. The Sudbury Neutrino Observatory. 1999. *arXiv:nucl-ex/9910016*.

[19] SNO Collaboration. A Search for Astrophysical Burst Signals at the Sudbury Neutrino Observatory. 2013. *arXiv:1309.0910 [astro-ph.SR]*.

[20] C.L. Cowan, F. Reines, F.B. Harrison, H.W. Kruse, and A.D. McGuire. Detection of the free neutrino: A Confirmation. *Science*, 124:103–104, 1956.

[21] G. Danby, J.M. Gaillard, Konstantin A. Goulianos, L.M. Lederman, Nari B. Mistry, and et al. Observation of High-Energy Neutrino Reactions and the Existence of Two Kinds of Neutrinos. *Physical Review Letters*, 9:36–44, 1962.

[22] D.Fargion. Detecting Solar Neutrino Flares and Flavors. *arXiv:hep-ph/0312011*.

[23] D.Fargion and P. Di Giacomo. Detecting Solar Neutrino Flare in Megaton and km^3 detectors. *arXiv:0812.4592 [astro-ph]*.

[24] D.M.Webber. An Improved Measurement of Electron Antineutrino Disappearance at Daya Bay. 2012. *arXiv:1211.1609 [hep-ex]*.

[25] Sophie Van Eck. Spectrophysique et Atmosphère Stellaires. Academic year 2013-2014.

[26] B. Adeva et al. A Direct determination of the number of light neutrino families from $e^+e^- \to \nu\bar{\nu}\gamma$ at LEP. *Physics Letters B*, B275:209–221, 1992.

[27] B. T. Cleveland et al. Measurement of the Solar Electron Neutrino Flux with the Homestake Chlorine Detector. *Astrophysical Journal*, 496:505–526, 1998.

[28] J. Beringer et al. Review of particle physics. Particle Data Group. *Physical Review D*, 86:010001, 2012.

[29] Kaoru Hagiwara et al. Review of particle physics. Particle Data Group. *Physical Review D*, 66:010001, 2002.

[30] E. Fermi. An attempt of a theory of beta radiation. *Zeitschrift für Physik*, 88:161–177, 1934.

[31] F.Halzen. High-energy neutrinos, January 2014. 1st Mercur Winter School on Plasma-Astroparticle Physics.

[32] F.Halzen and S.R.Klein. Invited Review Article: Icecube: An instrument for neutrino astronomy. *Review of Scientific Instruments*, 81:081101, 2010.

[33] L. Fletcher, B.R.Dennis, H.S.Hudson, S.Krucker, K.Phillips, A.Veronig, M.Battaglia, L.Bone, A.Caspi, Q.Chen, P.Gallagher, P.T.Grigis, H.Ji, W.Liu, R.O.Milligan, and M.Temmer. An Observational Overview of Solar Flares. *arXiv:1109.5932 [astro-ph.SR]*.

[34] D. Chirkin for the IceCube collaboration. Study of South Pole ice transparency with Icecube flashers. *Available on IceCube*.

[35] G.Drexlin, V.Hannen, S.Mertens, and C.Weinheimer. Current Direct Neutrino Mass Experiments. 2013. *arXiv:1307.0101 [physics.ins-det]*.

[36] G.Kowal, E.M.de Gouveia Dal Pino, and A.Lazarian. Magnetohydrodynamics Simulations of Reconnection and Particle Acceleration: three-dimensional effects. *The Astrophysical Journal*, 735:102–111, 2011.

[37] Kael Hanson. Astroparticles Physics course. Academic year 2012-2013.

[38] K. S. Hirata, T. Kajita, T. Kifune, K. Kihara, M. Nakahata, K. Nakamura, S. Ohara, Y. Oyama, N. Sato, M. Takita, Y. Totsuka, and Y. Yaginuma. Search for Correlation of Neutrino Events with Solar Flares in Kamiokande. *Physical Review Letters*, 61(23):2653–2656, December 1988.

[39] K. Hoshino. Result from DONUT: First direct evidence for tau-neutrino. In *APPC2000 Conf. Proc.*, page 58–63, 2000.

[40] J. R. Hörandel. Models of the Knee in the Energy Spectrum of Cosmic Rays. *arXiv:astro-ph/0402356*.

[41] I.G.Usoskin, K.Mursula, R.Arlt, and G.A.Kovaltsov. A solar cycle lost in 1793–1800: Early sunspot observations resolve the old mystery. *Astrophysical Journal*, 700:L154–L157, 2009.

[42] J.A.Miller. Particle Acceleration in Impulsive Solar Flares. *Space Science Reviews*, 86:79–105, 1998.

[43] J.F.Drake, M.Swisdak, H.Che, and M.A.Shay. Electron acceleration from contracting magnetic islands during reconnection. *Nature*, 443:553–556, 2006.

[44] J.P.Dumm. *A Searches for Point-like Sources of Neutrinos with the 40-String IceCube Detector.* PhD thesis, University of Wisconsin – Madison, 2011.

[45] J.Steinacker, W.Dröge, and R.Schlockeiser. Particle Acceleration in Impulsive Solar Flares. *Solar Physics*, 115:313–326, 1988.

[46] M. Karlicky and T.Kosugi. Acceleration and heating processes in a collapsing magnetic trap. *Astronomy & Astrophysics*, 419:1159–1168, 2004.

[47] K.Kotera and A.V.Olinto. The Astrophysics of Ultrahigh Energy Cosmic Rays. *arXiv:1101.4256 [astro-ph.HE]*.

[48] L.Fletcher, R.Turkmani, H.S.Hudson, S.L.Hawley, A.Kowalski, A.Berlicki, and P.Heinzel. Solar Flares and the Chromosphere. *arXiv:1011.4650 [astro-ph.SR]*.

[49] L.Fletcher, R.Turkmani, H.S.Hudson, S.L.Hawley, A.Kowalski, A.Berlicki, and P.Heinzel. Solar Flares and the Chromosphere. *arXiv:1011.4650 [astro-ph.SR]*.

[50] M.Danninger. *Searches for Dark Matter with IceCube and DeepCore. New constraints on theories predicting dark-matter particles.* PhD thesis, Stockholm University, 2013.

[51] K. Nakamura, T. Kajita, M. Nakahata, and A. Suzuki. Kamiokande. pages 249–387, 1994.

[52] N. Omodei and V. Petrosian. Fermi-LAT Observation of Impulsive Solar Flares. *Fermi Symposium Monterey*, 2012.

[53] M. Ossendrijver. The solar dynamo. *The Astronomy and Astrophysics Review*, 11:287–367, 2003.

[54] W. Pauli. Dear radioactive ladies and gentlemen. *Physics Today*, 31N9:27, 1978.

[55] D. H. Perkins. *Particle Physics and Cosmologie: The Interface*, volume Second Edition of *Oxford Master Series in Particle Physics, Astrophysics, and Cosmology.*

[56] Martin L. Perl, G.J. Feldman, G.S. Abrams, M.S. Alam, A. Boyarski, and et al. Properties of the Proposed tau Charged Lepton. *Physics Letters B*, B70:487, 1977.

[57] T. Pierog and D. Heck. CORSIKA an Air Shower Simulation Program. *Karlsruhe Institute of Technology website*.

[58] Fermi GI program. *http://hesperia.gsfc.nasa.gov*.

[59] R. Ramaty. Nuclear Processes and Accelerated Particles in Solar Flares. *Solar Physics*, 113:203–215, 1987.

[60] R.Boyle. Forget the Higgs, neutrinos may be the key to breaking the Standard Model. 2014. *http://arstechnica.com/science/2014/04/forget-the-higgs-neutrinos-may-be-the-key-to-breaking-the-standard-model/*.

[61] R.J.Protheroe and R.W.Clay. Ultra High Energy Cosmic Rays. *arXiv:astro-ph/0311466*.

[62] R.P.Litchfield. (Direct) Measurement of θ_{13}. 2012. Invited talk at Flavor Physics and CP Violation (FPCP 2012), Hefei, China, May 21-25, 2012. *arXiv:1209.3884 [hep-ex]* .

[63] S.A.Bogachev and B.V.Somov. Comparison of the Fermi and Betatron Acceleration Efficiencies in Collapsing Magnetic Traps. *Astronomy Letters*, 31(Issue 8):537–545, 2005.

[64] NOAA / Space Weather Prediction Center. *http://www.swpc.noaa.gov*.

[65] S.V.Hickford. *A Cascade Analysis for the IceCube Neutrino Telescope*. PhD thesis, University of Canterbury, 2012.

[66] T.Burgess. *A search for Solar Neutralino Dark Matter with the AMANDA II Neutrino Telescope.* PhD thesis, Stokholm University, 2008.

[67] Catherine Vander Velde. Détection de particules, acquisition et analyse de données. Academic year 2013-2014.

[68] Catherine Vander Velde. Interactions fondamentales et particules. Academic year 2012-2013.

[69] V.V.Zharkova, K.Arzner, A.O.Benz, P.Browning, C.Dauphin, A.G.Emslie, L.Fletcher, E.P.Kontar, G.Mann, M.Onofri, V.Petrosian, R.Turkmani, N.Vilmer, and L.Vlahos. Recent Advances in Understanding Particle Acceleration Processes in Solar Flares. *Space Science Reviews*, 159:357–420, 2011.

[70] W.C.Haxton, R.G.Hamish Robertson, and A.M.Serenelli. Solar Neutrinos: Status and Prospects. 2012. *arXiv:1208.5723 [astro-ph.SR]*.

[71] W.N.Cottingham and D.A.Greenwood. An Introduction to the Standard Model of Particle Physics - second edition. 2001.